

# Verification of Late Miocene to Quaternary structural control on landforms: a case study with comprehensive methodology from a low hilly area (western Pannonian Basin)

Gábor KOVÁCS<sup>1,2,3\*)</sup>, László FODOR<sup>4)</sup>, Szilvia KÖVÉR<sup>4)</sup>, Gábor MOLNÁR<sup>4)</sup>, Donát RAÁB<sup>1)</sup>, Tamás TELBISZ<sup>5)</sup> & Gábor TIMÁR<sup>1)</sup>

<sup>1)</sup> Department of Geophysics and Space Sciences, Eötvös University, H-1117 Budapest, Pázmány Péter sétány 1/C, Hungary;

<sup>2)</sup> Department of Geology, University of West Hungary, H-9700 Szombathely, Károlyi Gáspár tér 4., Hungary;

<sup>3)</sup> Geomega Ltd., H-1095 Budapest, Mester utca 4., Hungary;

<sup>4)</sup> MTA-ELTE Geological, Geophysical and Space Science Research Group, Hungarian Academy of Sciences at Eötvös University, H-1117 Budapest, Pázmány Péter sétány 1/C, Hungary;

<sup>5)</sup> Department of Physical Geography, Eötvös University, H-1117 Budapest, Pázmány Péter sétány 1/C, Hungary;

\* Corresponding author, skovacs.gabor@caesar.elte.hu

**KEYWORDS** Pannonian Basin; structural control; electrical resistivity tomography; Rechnitz window; post-rift faulting; Miocene

## Abstract

The transition zone between the subsiding western Pannonian Basin and the uplifting Eastern Alps is a slightly undulating hilly realm, consisting of large plateaus, pediment surfaces and locally steep scarps. These rectilinear slopes are considered as being controlled by structural elements as suggested by the digital elevation model (DEM), although a simple denudation origin cannot be ruled out from surface data only. One of the steep slopes, the Torony scarp is situated E from the Eisenberg-Vas Hill and was investigated with diverse methods: 2D electric tomography, 1D electric resistivity data, correlation of borehole data and fault-slip analysis. The dense network of shallow boreholes and the applied geophysical methods constraints well the structural geometry of the Upper Miocene (Pannonian) lignite layers. While Miocene layers were only very slightly tilted away from the Torony scarp, they are faulted and folded just below the scarp. Correlation of layers on both sides of the scarp is not unequivocal, thus the exact total vertical displacement can only be estimated between 25-50 meters.

Observations are in agreement with the assumptions based on the DEM: the Torony segment of the Arany creek is controlled by a fault system. The fault system is composed of two sets: a NE–SW and one (W)NW–(E)SE striking. The former can be interpreted as an echelon faults, while the latter set as connecting fault splays between the main echelon segments. Outcrop-scale observations revealed partly syn-sedimentary Late Miocene and partly younger normal faulting. Based on the age of the underlying sedimentary units the Torony fault system could not start earlier than 8.7 Ma, most probably at 8.3 Ma. On the other hand, the deformation partly post-dates the Late Miocene layers. Depending on correlation of lignite strata across the fault zone and on the concept on the denudation process, the post-sedimentary part of faulting could be pre-Quaternary or Quaternary. Presence of active mass movements and deeply eroded gullies suggest that the slope is still unstable; this may be an indirect indication of fault-controlled slope development. The Torony fault is part of a system of Late Miocene or younger faults which partly reactivated, partly dissected the earlier syn-rift (late Early to Mid-Miocene) faults of the western Pannonian Basin. Besides the structural results, this paper emphasizes the advantage and necessity of simultaneous usage of geophysical measurements, field observations, morphological investigations and borehole data.

## 1. Introduction

Steep, rectilinear slopes are frequently considered as being controlled by structural elements. A number of studies automatically take the linearity of landforms as prove for structural, most frequently fault control. However, this logical but not unequivocal conclusion needs careful verification, because diverse geomorphic process alone can also result in straight valley sides, river stretches etc. Among others, glacial erosion, wind abrasion, river erosion, all produces linear landforms (Nash and Beaujon, 2006; Pelletier et al., 2006). Structural control on such landforms can be difficult to prove, because of poor outcrop conditions, and the lack of adequate surface and subsurface data sets. It is particularly true for landforms within the Pannonian Basin, central Europe, which offers poor

outcrops for both geological and geomorphological analyses, landforms are vegetated and sometimes anthropogenically modified.

Structural control can be derived from either inherited elements (Berry et al., 1990; Colella et al., 2004; Alasset and Meghraoui, 2005; Fubelli et al., 2009; Štěpančíková et al., 2011) or active deformation (Marple and Talwani, 2000; Zovoili et al., 2004; Alasset and Meghraoui, 2005). In the former case, the controlling structural element was formed before the time of the given landscape evolution phase. Diverse denudation processes can passively exhume the structure (Petit and Mouthereau, 2012), which, on its two sides, has rocks with different resistance against erosion which may lead to contrasting rate

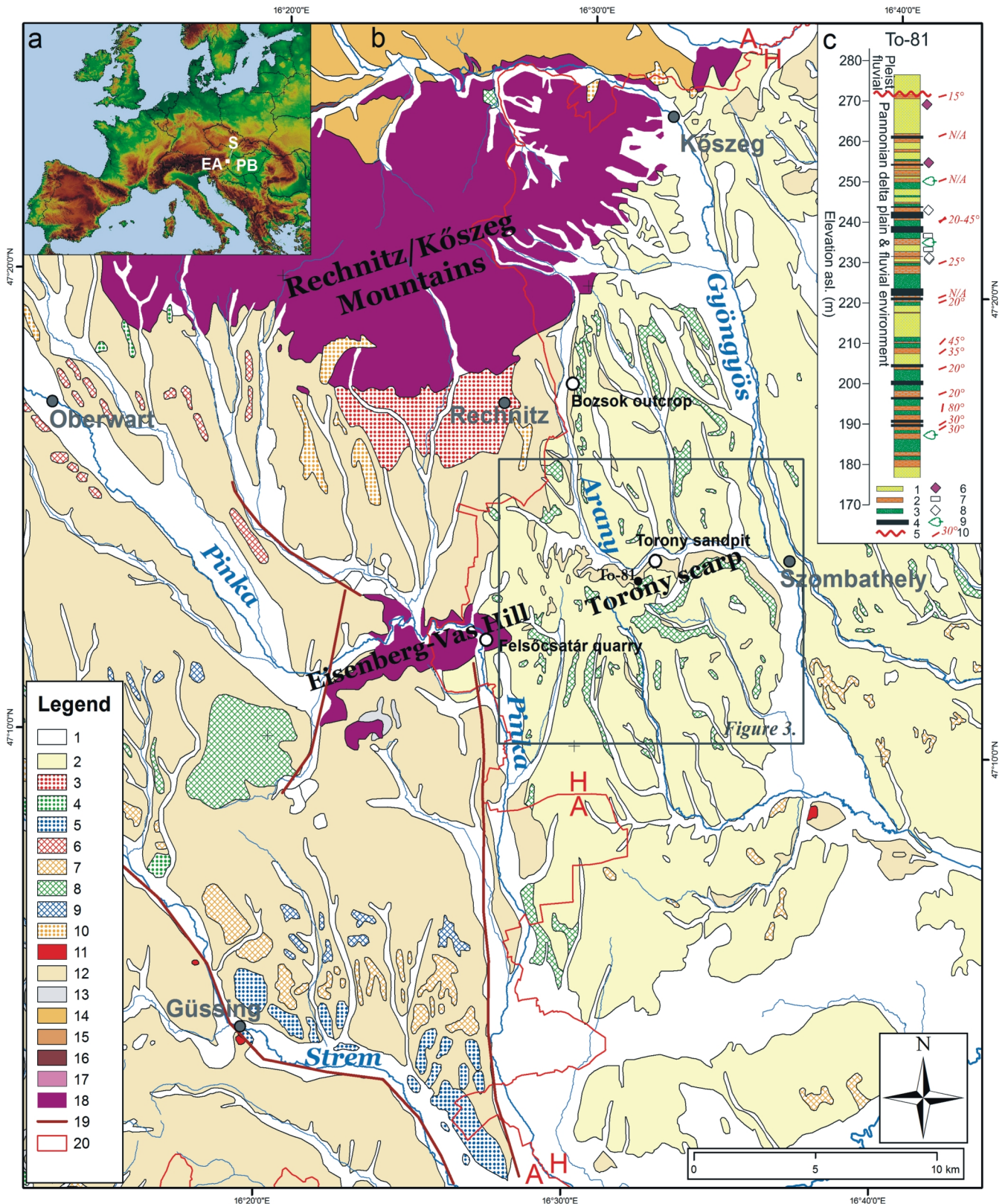


**Figure 1:** a) Location of the study area. EA – Eastern Alps; PB – Pannonian Basin; S – study area. b) Geological map of the study area (according to Pascher, 1999). Hungarian terrace classification: H, Austrian terrace classification: A. 1 – Holocene fluvial sediment; 2 – loess; 3 – gravelly slope debris; 4 – gravel terrace: Middle–Upper Pleistocene (H: IIb, A: V); 5 – gravel terrace: Middle Pleistocene (H: III, A: IV), 6 – gravel terrace: Middle Pleistocene (A: IIIa); 7 – gravel terrace: Lower–Middle Pleistocene (H: IV, A: IIIb); 8 – gravel terrace: Lower Pleistocene (H: V, A: II), 9 – gravel terrace: Lower Pleistocene (H: VI, A: I); 10 – gravel: Upper Pliocene–Lower Pleistocene; 11 – Cenozoic basaltic volcanics (Pliocene–Pleistocene tuff and Pannonian–Sarmatian basalt); 12 – Pannonian sediment (sand, clay, gravel); 13 – Upper Pannonian travertine; 14 – Sarmatian sediment (sand, clay, gravel); 15 – Carpathian sediment (sand, clay, gravel); 16 – Ottnangian sediment; 17 – Upper Austroalpine nappe units; 18 – Penninic unit; 19 – Supposed faults, according to Nebert (1979); 20 – National border. White-black circles refer to field observation spots. c) Lithology of the study area and example for data used for correlation based on To-81 borehole. 1 – sand; 2 – clay; 3 – silt; 4 – lignite; 5 – discordance; 6 – limonite concretions; 7 – calcareous layer; 8 – carbonate concretions; 9 – organic layer or biogenic remnants; 10 – observed fault plane with dip angle.

outcrops for both geological and geomorphological analyses, landforms are vegetated and sometimes anthropogenically modified.

Structural control can be derived from either inherited elements (Berry et al., 1990; Colella et al., 2004; Alasset and Meghraoui, 2005; Fubelli et al., 2009; Štěpančíková et al., 2011) or active deformation (Marple and Talwani, 2000; Zovoili et al., 2004; Alasset and Meghraoui, 2005). In the former case, the controlling structural element was formed before the time of the given landscape evolution phase. Diverse denudation processes can passively exhume the structure (Petit and Mouthereau, 2012), which, on its two sides, has rocks with different resistance against erosion which may lead to contrasting rate of denudation in the two fault blocks. In that scenario, the spatial coincidence, similarity in direction of the older structural element and the landform should be pointed out. Demonstration of active (neotectonic) control on landform can be more complicated, while the young age of deformation could be hard to prove. Although a number of geomorphic indices can be evaluated and used as indications for active deformation, undoubted demonstration of the age of the structure and thus the controlled landform remains elusive.

Demonstration of structural control on a specific landform may involve various methods and data sets. In one successful example from the Pannonian Basin, Ruszkiczay-Rüdiger et al. (2007, 2009) used complex surface and subsurface data sets to infer structurally constrained landforms. Štěpančíková et al. (2011) distinguished the usage of different scaled methods of fault designation and detailed investigation.

In our study we partly follow this line of combined methodology, but use different subsurface and surface data sets. Instead of a network of seismic reflection data, we used other types of geophysical methods, namely 2D electric tomography and 1D electric resistivity data. Relatively dense network of shallow boreholes permitted the construction of cross sections and could be compared to geophysical data. Finally, surface fault-slip data proved important for characterisation of fault geometry and fault kinematics. All these data permitted to build a 3D model for the studied drainage anomaly, the sharp bend of the Arany creek in front of the Torony scarp, located in the western Pannonian Basin, at its transition to the Eastern Alps (Fig. 1a). The combined data set suggests that an echelon normal or oblique-normal faults controlled linear ENE trending segments, which is almost perpendicular to the general SSE directed flow direction of the drainage network, including the upper reach of the Arany creek.

## 2. Geological setting

The pre-Cenozoic basement of the study area consists of different Alpine nappes. In the outcrops of the Rechnitz-Kőszeg Mts. and Eisenberg-Vas Hill different slices of the Upper Penninic unit are present. It consists of two main complexes: (1) serpentinised ultramafic, metagabbro, greenschist and blueschist rock-association; (2) metasedimentary complex with calcareous phyllite, quartz-phyllite and meta-conglomerate

(Koller and Pahr, 1980). Geochemical data indicate high Ti ophiolitic character (Koller and Pahr, 1980) formed at a well-developed middle oceanic ridge system. For the metasedimentary complex the supposed range of sedimentation is from Early Jurassic to Late Cretaceous, although only the mid-Cretaceous is proven by Schönlaub (1973) based on sponge spicules.

Above the Penninic unit, thin slices of the Austroalpine nappes occur both on the NW side of the Eisenberg-Vas Hill and on the south-eastern slope of the Bernstein Penninic window to the NW of the investigated area (Pascher, 1999). The Lower Austroalpine nappe comprises the Wechsel series and belongs to the Lower Austroalpine nappe-stack (Schönlaub, 2000; Schmid et al., 2004). The upper slice belongs to the Upper Austroalpine nappe –system according to the new definitions of Schmid et al. (2004).

The oldest post-Mesozoic cover sediments occur only in the deep half grabens: late Early Miocene (Karpatian) gravel, sand, silt and Middle Miocene clastics were deposited in terrestrial to marine settings (Kisházi and Ivancsics, 1981, Vendel, 1973). Middle Miocene marlstone and siltstone only occur east from the study area, in syn-tectonic half grabens. The much more extensive cover, the Late Miocene (Pannonian) consists of silt, clay and sand strata (Fig. 1b, c). During the Late Miocene sedimentation, the evolution of the basin fill followed the general trend of the Pannonian Basin (see Szentgyörgyi and Juhász, 1988, Juhász et al., 1999, Magyar et al., 2007, Sztanó et al., 2013), having evolved from deep lake through shelf slope, to delta and finally to delta plane and fluvial environment. In these latest periods the area was a marsh zone where clayey, sandy and silty layers with thin lignite horizons deposited. If the lake level rose, somewhat coarser-grained sediment, sand or silty marl formed. This alternating sedimentation motif provides the opportunity to follow key horizons between boreholes and by geophysical methods.

The deltaic to fluvial Pannonian strata are covered, after an unconformity surface, by Quaternary fluvial and aeolian formations (Fig. 1c). These young sediments are generally covered by extensive soil blanket, however, they crop out along the steep morphological scarps of the area. The oldest few dm to m thick Quaternary sediment is gravel, which is widespread with varying thickness. Physical features like coatings of the gravelly sediment are not uniform in the wider area. Such differences are considered as indicators of relative age of the Pleistocene sediment and were used to differentiate terrace levels nearby to the study area by Hermann (1990), between Pinka and Strem rivers (Fig. 1b). Pleistocene sediments on both side of Torony scarp are different. N from the scarp light yellow gravelly clay occurs without pebble coating, while in the south pebbles are coated with reddish desert varnish. Gravels are often buried by atypical aeolian loess (Eicher, 1994, Fekete, 2011, Fekete and Kovács, 2012). The bottoms of wide, fluvial valleys are filled by Holocene sediments (Pascher, 1999).

## 3. Geomorphology

Generally, the wider study area can be divided into two parts

by the lower course of the river Pinka. East of this line, there is a low hilly landscape consisting of small plateau-like terrains tilting towards SE (Fig. 2a, b; Pinka Upland, Rechnitz Mountains' Foothill and Gyöngyös Upland). Both drainage density and relative relief are generally low within this part (Fig. 2a, relative relief is 10-20 m –calculated as the elevation range within a 500 m circle). Flat plateaus are dissected by several 10-40 m deep valleys (Fig. 2c, d, e). N-S swath profile of the

area (Telbisz et al., 2013) reveal the southward flattening of the plateaus (Fig. 2g). Units S from the plateaus can be characterized with extremely flat surface: mode of slope calculated in 500 m radius circle is lower than 0.5° (Fig. 2b), tilting of envelope surface fitted to swath profile is maximum 0.08° (Fig. 2g) and slope histogram shows an extreme peak of max. 1° (Fig. 2j). Northward the tilting of envelope surface reaches 0.75° (Fig. 2g), mode of slope locally reaches 2-3° (Fig. 2b) and

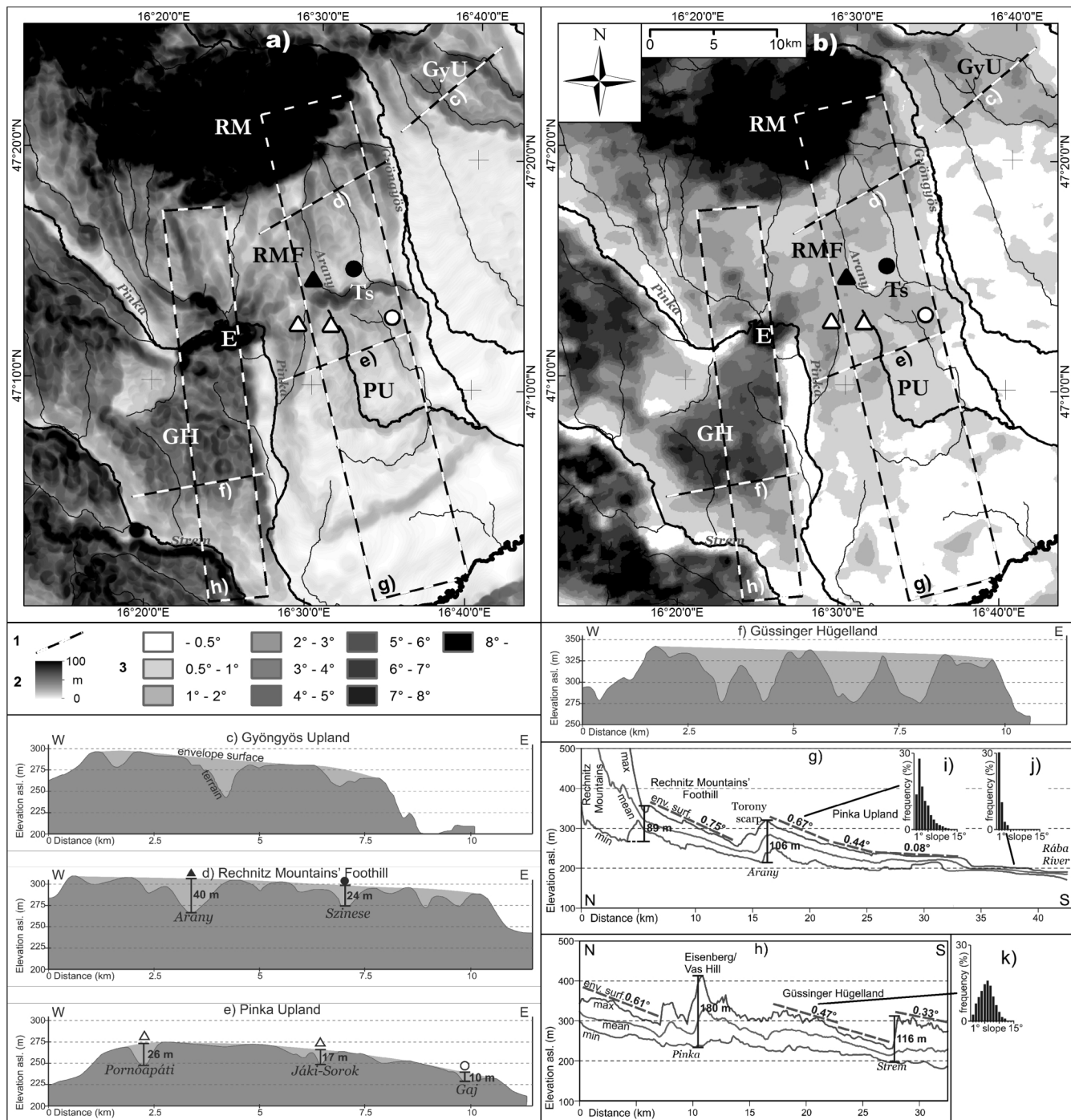


**Figure 2:** Geomorphology of the study area. 1 – location of profiles and swath profiles with the letter of inset; 2 – grey shading for relative relief (inset a); 3 – colors of mode of slope values (inset b). Insets: a) Relative relief. b) Mode of slope. c–f) Topographic profiles with the fitted envelope surfaces and valley incisions (for location see a & b inset). g–h) Swath profiles with scarp heights, fitted envelope surfaces and their dip angle (for location see a & b inset). i–k) Slope histograms of some units. E: Eisenberg-Vas Hill, RM, RMF: Rechnitz Mountains, Rechnitz Mountain Foothills; GH, PU, GyU: Güssinger Hügelland, Pinka, Gyöngyös Upland, Ts: Torony scarp.

the most dominant slope value of the whole Pinka Upland become 1–2° (Fig. 2j). The principal SSE drainage direction are not perfectly controlled by the dominant aspect. At many locations, secondary ENE-directed streams (e.g. the lower course of Arany, the central course of Pinka) cut the main NNW–SSE trend. These streams have asymmetric valleys with gently dipping northern sides and steeper southern slopes like the investigated Torony scarp (Fig. 2g, h).

Some valleys seem to be the downstream continuation of upper reaches occurring on the neighbouring plateaus. On the Pinka Upland, Pornóapáti and Jáki-Sorok creeks are flowing southward from the Torony scarp as the continuations of the southward flowing section of the Arany creek (marked with triangles in Fig. 2a, b, d, e). To the east, the Gaj creek of Pinka Upland seems to be the southward continuation of the Szinese creek (marked with circles in Fig. 2a, b, d, e). Eastward decreasing valley depths in both plateaus, the fact that incision is higher in Rechnitz Mountains' Foothill than in Pinka Upland and observed wind gaps previously led Kovács and Telbisz (2013) and Kovács et al. (2014) to reconstruct drainage network changes triggered by the uplifting Torony scarp.

West of the lower course of the Pinka river (Fig. 2a, b; Güssinger Hügelland), the terrain is more uplifted (by ~50 m) with much higher relief (mean relative relief is ~50 m) and intense fluvial dissection. Plateau-like character is not observable neither on elevation models and derived maps (Fig. 2a–b), nor on E–W topographic survey (Fig. 2f), nor on the slope histogram (Fig. 2k). However, slightly tilted plains can be fitted to the ridges between incised streams (Fig. 2f). Curves of topographic swath survey (Fig. 2h) are less smooth than on the eastern part (Fig. 2g) due to the high-rate linear erosion. However, more or less the same tilted envelope surfaces can be fitted to the maximum curve as on the eastern side. The overall view is the same: the surface is getting more tilted approaching Rechnitz-Kőszeg Mountains and Eisenberg-Vas Hill. Drainage directions are mostly N–S and NW–SE. In many river valleys, southern and southwestern sides are steep, whereas northern and northeastern sides are less steep (Pinka and Strem rivers; Fig. 2a). One of these steep valley sides, the Torony scarp, is investigated in this study.

The lower part of the scarps is covered by colluvial sediments that were formed recently by still active geomorphologic movements, such as landslides and slope creep. Small creek fans and narrow but relatively deep gorges also contributed to the formation of the scarps. The activity of the above phenomena suggests the recent instability of the scarp. It may have caused either by recent tectonic activity or by the exhumation of presently inactive faults (Gallousi and Koukouvelas, 2007; Fubelli et al., 2009; Goswami et al., 2011; Dill et al. 2012). Landslides corresponding to supposed faults were observed and described in the neighbouring Middle Burgenland by Fellner and Hermann (1993). According to their work, along most parts of the asymmetric valley of the Strem River both relatively old, stable landslides as well younger secondary slides occur. Similar landforms are depicted on the geological

map (Herrmann et al., 1993) along the southern scarp of Pinka Valley. Both valleys have supposed fault-related segments by Nebert (1979).

## 4. Methods

### 4.1 Boreholes

The study area is surveyed by densely drilled (2–300 m) boreholes targeting the underground lignite reserves. The borehole data is accessible at the Hungarian Geological, Geophysical and Mining Database. The borehole dataset consists of coordinates, elevation, bottom depth and identifier of each borehole. It was used to create a GIS database in order to construct cross section profiles (Fig. 3). Directions of profile lines were designated by using closely spaced and similar depth boreholes to reach a successful correlation of lignite layers. On the other hand, lignite layers were correlated laterally, among different profiles, too. When continuity of lignite-bearing strata cannot be constructed, we established a fault indication, indicated by letter *f* in the order of their appearance in the text. If such indications can be correlated along strike, using other profiles or geophysical data, we suggest the presence of a fault, designated with letters *F*. The amount of displacement depends on the correlation of layers between the adjacent fault blocks. In some cases this correlation is not unequivocal; in this case we indicated two possible correlation solutions.

Electric sounding data of boreholes (showing differences in layer resistivity) was also used to outline geophysical profile locations (Fig. 3).

Penetrated successions of boreholes (Fig. 3) were classified into the following lithologies: lignite, clay, sand, silt, marl and siltstone, gravel (example is given on Fig. 1c). Depth of the Pannonian–Quaternary boundary was also established. Marl and siltstone occurrences are very sparse, while gravel occurred only in Quaternary sediments. Due to the long period of the drilling campaign (1941–1989) and different explanatory experts, significant bias occurs in lithological characterisation of adjacent boreholes. Despite this difficulty, sediments near the lignite, especially clay and sand, were useful for more accurate correlation of the lignite layers between boreholes. In our profiles only the lignite layers and the Pannonian–Quaternary boundary are presented for the sake of clarity (Fig. 4–8). Lignite outcrops observed by Jaskó (1947) were used and placed in profiles. Dip angles of the lignite layers remain minor, generally below 2°. This value was obtained by the correlation of the same layer across several boreholes; in the southern part of the study area, where layers are not cut by faults thus dip degree determination is possible.

### 4.2 Electric methods

During our field campaign, several geophysical methods were used to depict the Neogene–Quaternary formations. Some of the results were described by Bereczki et al. (2013) mainly focusing on the pre-Cenozoic basement geometry, while others are described here. 2D geoelectric tomography using multi-

electrode resistivity metre (MUEL) and 1D vertical electric sounding (VES) were used to detect the geometry and possible ruptures of the Upper Miocene sedimentary layers (Fig. 3). With the surface geoelectric methods the electromagnetic field properties of the subsurface layers were determined (Lowrie, 2007). The geometry and lithology of near-surface layers are defined on the basis of their different electric characteristics. Direct current geoelectric surveys aimed determination of resistivity. The best conductors, which are characterised by lowest values, are clays and marls containing considerable amount of bound water within the rock matrix (Lowrie, 2007). Ground water level was observed to be only few meters (max. 2 m) below the ground in the whole study area. Thus results of geoelectric measurements are not modified by the effects of the lower conductivity of strata above ground water surface. The range of resistivity varies over orders of magnitudes, thus there is no specific value for certain rock

types. However, where geologic data suggests contrast in the resistivity values, geoelectric methods proved to be suitable tools to delineate different lithological units (Dombrádi 2012) or faults with vertical component (Caputo et al. 2003; Štěpaňčíková et al. 2011). The applied MUEL array was Wenner-Schlumberger, the minimal electrode spacing was 4 m and the total length of one measurement was 124 m. The interpreted profile was the inversion result of 5 iterations, with 0.88% standard deviation.

### 4.3 Fault-slip analysis

Field structural work comprised the observation and measurement of brittle structural elements, e.g. joints, faults and striated fault planes. This latter permitted the calculation of the paleostress axes, using the approach of Angelier (1984; 1990). In case of lack of striations we grouped the fractures (faults and joints) in apparently conjugate sets and then only

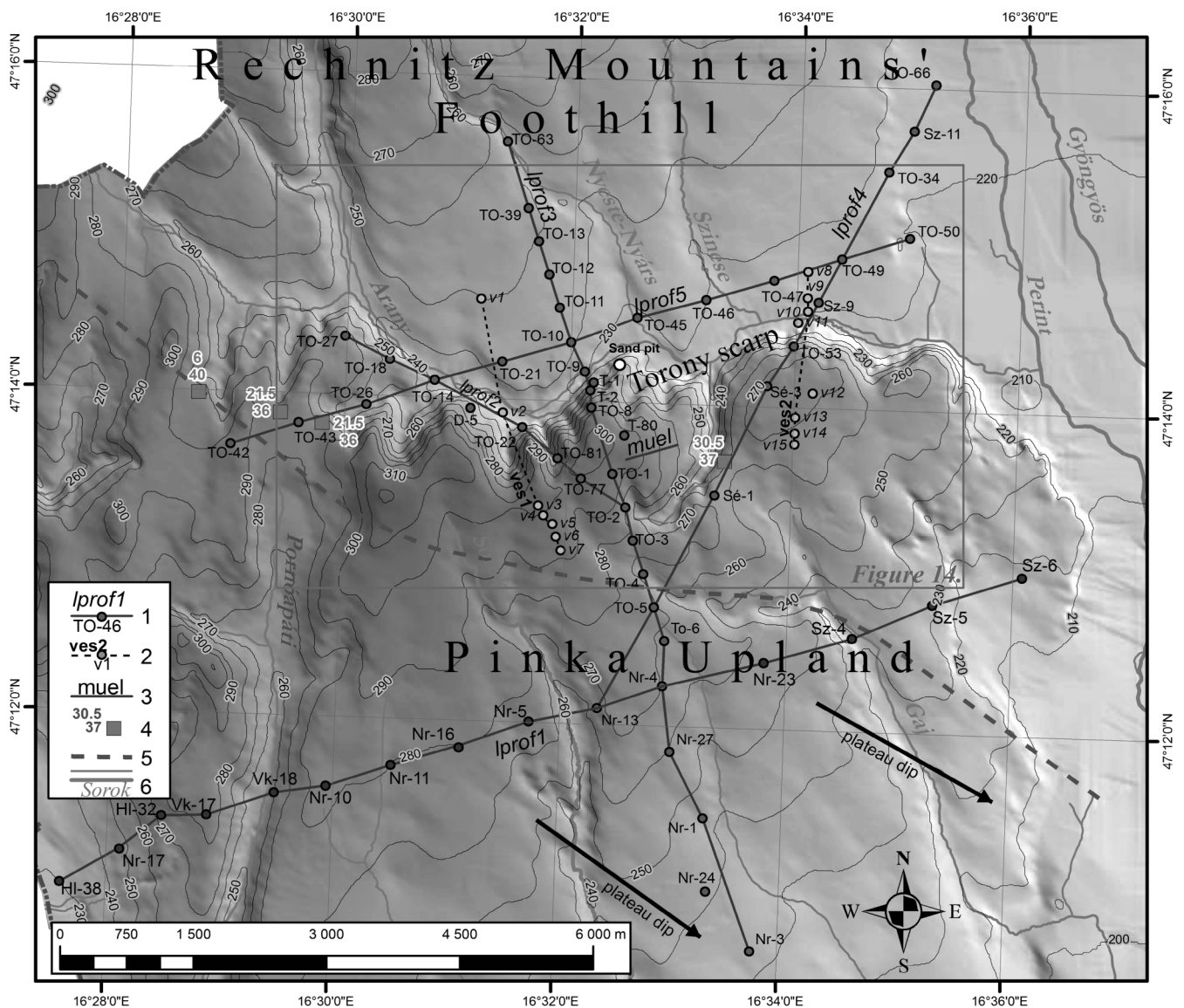


**Figure 3:** Overview of the study area. 1 – section profiles using borehole data; 2 – VES profiles; 3 – multielectrode profile of 2D resistivity tomography; 4 – previously determined wind gap (upper parameter denotes relative incision, lower denotes relative position to base level); 5 – vcsa-33 industrial seismic section; 6 – creeks. White-black circle refers to field observation spot.

estimated the stress axes using the hypothesis of Anderson (1951). Thickness difference between the footwall and hanging wall blocks was observed to check syn-sedimentary nature of faults.

## 5. Results

### 5.1 Geomorphologic observations

Large scale morphology of the area is presented in the introduction, in this chapter we focus on the investigated scarp. The Torony scarp is a significant morphological feature between the Rechnitz–Kőszeg Mts., Eisenberg-Vas Hill and Gyöngyös River. To the N, the slightly undulating southern foothill of the Rechnitz–Kőszeg Mountains gently dips to the south. South of the scarp, there is a slightly undulating hilly surface with a gentle dip towards SE (Fig. 3), which is called the Pinka Upland. Digital Terrain Model (DTM) of the study area clearly shows, that the scarp is not a straight line, but consists of almost perpendicular WNW–ESE and SW–NE segments.

The Torony scarp represents abrupt changes in the direction of creeks. Southward flowing creeks draining the water from Rechnitz–Kőszeg Mountains abruptly turn to the east along the scarp. The Arany creek follows the directions of the scarp segments, therefore its planform channel geometry shows low frequency curves (Fig. 1, 2 and 3). South from the scarp, the system of southward-flowing creeks continues, although the westernmost Pornóapáti creek has a slightly different direction. Flow direction of the creeks of the Pinka Upland differs from the general southeasterly dip of the upland itself (difference ~45–50°).

On the Pinka Upland the uppermost valley segments starting from the scarp are dry and without a valley head, these are wind gaps (marked as squares on Fig. 3; after Kovács and Telbisz, 2013). The first number (next to square symbols in Fig. 3) indicates the depth of the wind gap (that is an approxima-

tion of pre-capture incision), whereas the second number indicates the relative elevation of the wind gap (i.e. the approximate value of relative post-capture lowering of Arany creek). These landforms indicate that at least some of the creeks used to flow to the south continuously above the present location of the Torony scarp before being captured by the eastward flowing lower Arany creek.

Our earlier investigations (Kovács et al., 2008) proved that the Torony scarp has an unstable slope: landslides and small gorges dissect the escarpment, which is also shaped by creep process. The latter is a slow mass movement, which is clearly observable in the area of settlements: it creates ruptures in houses, leaning fences and pylons. Low-rate creeping is measurable on natural areas, too. These geomorphic processes occur only at the outcrop of Pannonian sediments, while gravel beds seemingly protect underlying layers from this type of denudation.

In the wider study area, abrupt changes in the orientation of certain creeks can be observed not only on morphologically constrained, but also on totally plain areas (Fig. 1). Note, that in some cases, these phenomena could have been caused by ancient Romans (Bödöcs et al. 2014).

### 5.2 Borehole data

In this section we discuss the cross sections based on borehole data. Particularly we focus on the dip attitude of lignite layers, and on the number, location and apparent dip direction of faults. Here we mainly note such locations, and their correlation with other indices is mostly discussed in chapter 6.1. Discussion on the consequences of alternative displacement solutions are addressed in the 6.4. chapter.

The *lprof1* section (Fig. 4; for location see Fig. 3) represents undisturbed layering below the Pinka Upland, on the southern part of the study area. In such case, the unfaulted lignite layers can obviously be correlated between neighbouring boreholes.

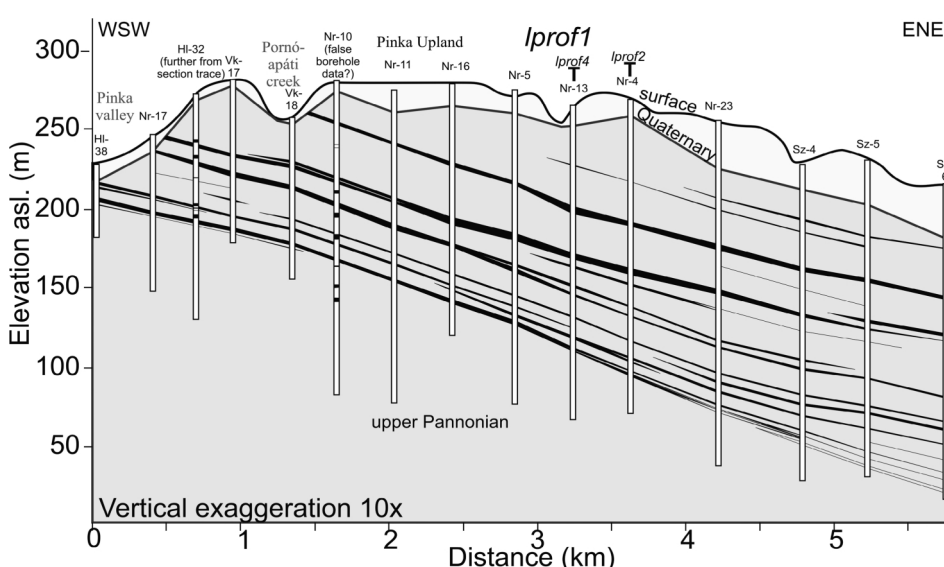


**Figure 4:** Section profile using borehole data (*lprof1*). Lignite layers are highlighted as black lines. Note the undisturbed layering on the southern side of the study area. For location see Fig. 3.

The number of lignite layers increase from 6 recognisable thick layers in the west to 12 thinner horizons in the east. This phenomenon is due to a slight change in depositional environment which was closer to the deep lake eastward (Juhász et al., 1999). The lignite layers might have a very gentle original depositional dip. However, the actual 1–2° is mostly the consequence of a regional tilt. This tilt is due to a more regional effect, the ongoing subsidence of the centre of the Danube basin, located further to the east. This gentle tilting can also has its origin due to neotectonic (Pliocene-Quaternary) structural inver-

sion, which resulted in differential uplift of margins of the Pannonian Basin (e.g. Eastern Alps) with respect to the basin centres (Horváth and Cloething, 1996).

The *lprof2* section (Fig. 5; for location see Fig. 3) crosses both the Arany creek and the Torony scarp at a very low angle. South-east from the escarpment, lignite layers seem to be continuous and dip southward, while at borehole TO-22 a displacement can be observed (fault indication *f01*). The downfaulted layers seem to continue up to borehole D-5 with the same southward dip. NW from borehole D-5 lignite layers cannot be connected with planar straight lines. Correlation of strata between To-27 and -18 boreholes suggests that dip direction changed to NW. This change in dip direction, and the position of lignite layer in borehole TO-14 may suggest the existence of two other fault indications: *f02*, and *f03*. Lignite outcrop along the scarp between TO-14 and D-5 also strengthen the applied structure. The entire section can be interpreted as a slight fold, faulted at its hinge zone; this structure is discussed later (6.2. chapter). The amount of displacement is poorly constrained by separated boreholes within individual fault blocks.

*lprof3* (Fig. 6) is the longest section that permits an overview of the general disposition of the lignite layers in a N-S section. Layers dip southward SSE from the scarp (from profile distance 3.5 km), and are horizontal at the escarpment (2.3-3 km), and gently dip to the NNW between 0-2.3 km. As a consequence, a slight updoming just N from the scarp can be observed. Layers are displaced significantly only

along the scarp; *f04* with ~15 (marked with triangles) or with ~50 m (marked with diamond) vertical drop. Similar faults were also observed in former mines (Jaskó 1947) and during our fieldworks as well (see chapter 5.4).

*lprof4* (Fig. 7) is a NE-SW profile that intersects the scarp. Layers are almost horizontal south from the escarpment, only a small downwarping can be observed at borehole Sé-1, which flattens upward. Layers are displaced twice at the scarp: between Sé-3 and TO-53 (with 60 m marked with rectangle or with only a few meters marked with circle; *f05*), and with 30-35 m between Sz-9 and TO-49 (*f06*). Strikingly, lignite layers with the same thickness have thicker sandy intercalations in TO-49 than in Sz-9 boreholes. This observation has bearing on correlation of displaced layers and also on their age; this will be exploited in chapter 6.3. Between Sz-11 and TO-66 a normal fault (*f07*, ~20-25 m) can also be recognized. Lignite layers N from the scarp dip northward, thus the section show

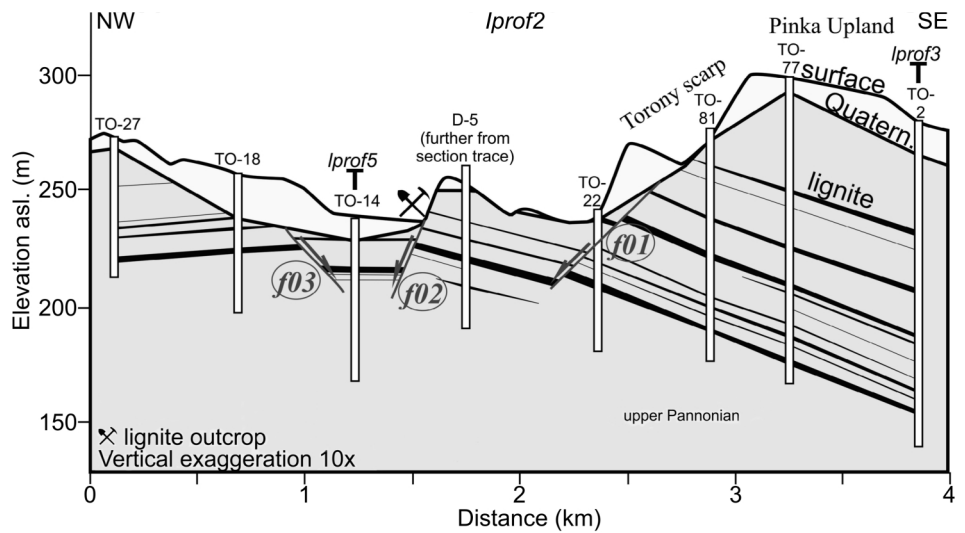


**Figure 5:** Section profile using borehole data (*lprof2*). Lignite layers are highlighted as black lines, which outcrop observed by Jaskó (1947) marked. For location see Fig. 3.

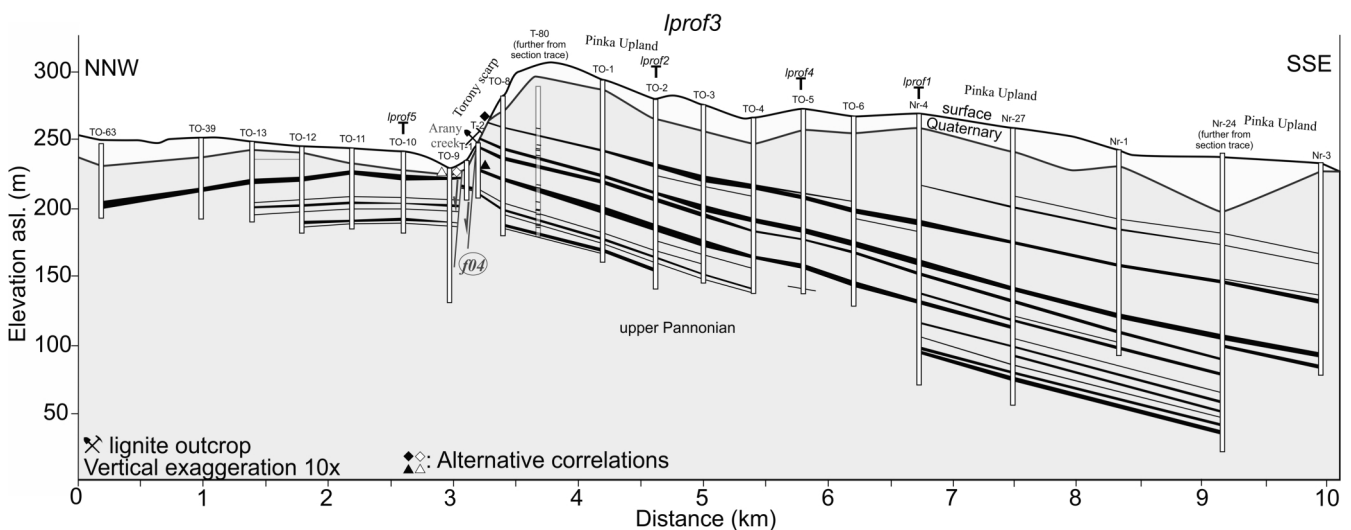


**Figure 6:** Section profile using borehole data (*lprof3*). Lignite layers are highlighted as black lines, which outcrop observed by Jaskó (1947) marked. For location see Fig. 3.

a gentle dome, similarly to profile 2 and 3.

*lprof5* (Fig. 8) is a W-E section that intersects the previously mentioned profiles. At the western end of the profile the lignite layers are almost horizontal, and are pinching out around TO-42 borehole. At the western side of TO-14 borehole the layers are faulted (*f08*), which corresponds well to the scarp at the right bank of the Arany creek.

Lignite layers are positioned lower in borehole TO-45 than in TO-21. The interpretation of the intermittent stratal geometry is not unequivocal. One can consider two faults with ca. 1-15 m throw at both sides of borehole TO-10. Alternative explanation would be the supposition of a monocline between the boreholes in question (see also the Discussion chapter). East from TO-47 a normal fault with ~34 m vertical drop is present (*f09*).

### 5.3 Geophysical data

The Torony scarp was investigated along several MUEL and two VES profiles. Since the penetration depth is lower than the scarp height, most MUEL sections could not provide enough information to follow resistivity horizons and detect possible fault indications using the available cable length. Only one

section was prepared at right angle to a secondary scarp south from Torony village (Fig. 9, for location see Fig. 3).

The overall view of the section with the applied vertical exaggeration (5×) present a low resistivity unit (<26 Ωm) thickening westward from 1 m to maximum 16 m. The underlying higher resistivity strata are very gently tilted eastward. Smoothing the rugged surface of the lower strata 1.2° dip angle can be reconstructed; this value corresponds well with dip data from borehole sections; see above. At around 280 m surface distance, a 5-6 m vertical drop of the higher resistivity strata can be observed (*f10*). We interpret this step as a sign for a fault. As we will suggest later, this small-displacement fault is a subsidiary element of the Torony scarp fault system.

In the research area VES proved to be more practical due to its deeper penetration in spite of its smaller resolution and point-like results. Seven measurements were carried out along *ves1* section crossing the main scarp, located between Dozmat and Torony villages (Fig. 3). Five measurements on the Pinka Upland provided similar resistivity distribution as MUEL profile (compare Figs. 9 and 10): 10-30 Ωm resistivity strata is underlain by higher resistivity sediment (30-50 Ωm). The boundary of resistivity is gently south-dipping and can be interpreted

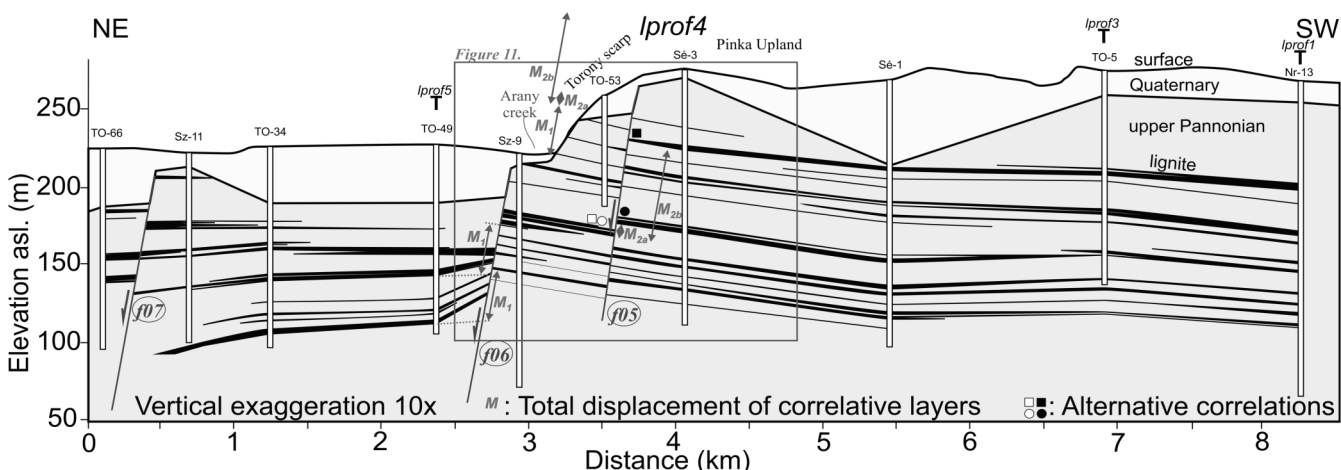


Figure 7: Section profile using borehole data (*lprof4*). Lignite layers are highlighted as black lines. For location see Fig. 3.

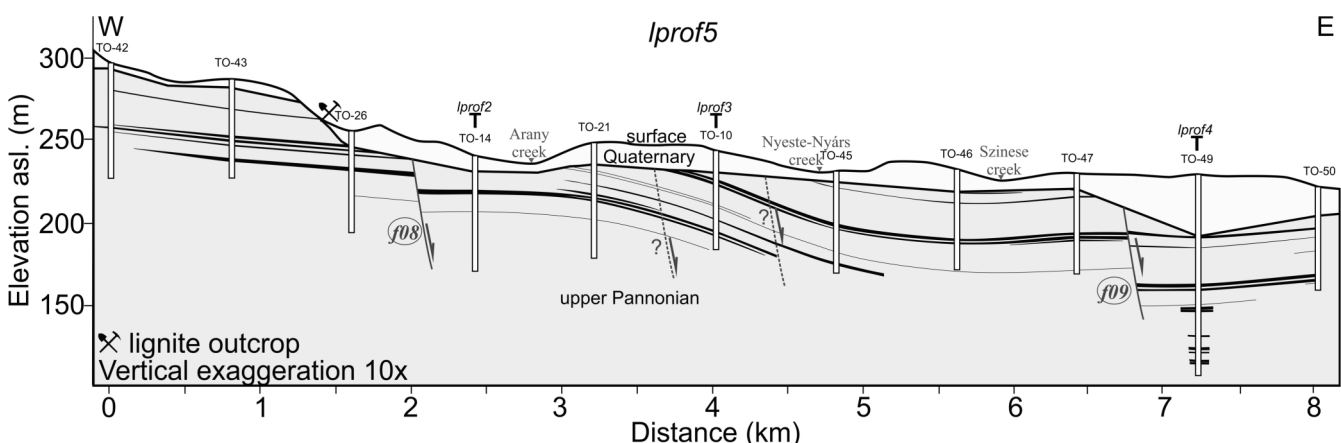


Figure 8: Section profile using borehole data (*lprof5*). Lignite layers are highlighted as black lines, which outcrop observed by Jaskó (1947) marked. For location see Fig. 3.

ted as a sedimentary unit boundary, probably between low resistivity clayey and somewhat higher resistivity sandy units. Measurements carried out on the alluvial plain of Arany creek, in front of the scarp, show similar results, though the lower strata show slightly higher resistivity (50-70  $\Omega\text{m}$ ). At the top  $v_2$  and  $v_1$ , a thin layer of higher resistivity sediment can be observed.

Ves2 section, including 8 measurements, also crosses the main morphological scarp. Four measurements on the Pinka Upland provide the following structure (Fig. 11): low (0-15  $\Omega\text{m}$ ) resistivity strata is underlain by higher resistivity sediment (45-80  $\Omega\text{m}$ ), that is underlain by a unit with intermediate 15-45  $\Omega\text{m}$  resistivity. Measurement  $v_{15}$  provides an extraordinary result: higher than 80  $\Omega\text{m}$  resistivity appear at the deepest section.

If a theoretical horizon is fitted to the bottom of the shallow high resistivity strata, 55-60 m drop can be observed along the scarp ( $f_{12}$ ). Another drop can be observed between  $v_8$  and  $v_9$ , but the amount of throw cannot be calculated due to the correlation difficulties of high resistivity strata of  $v_9-11$  and  $v_{12-15}$  (see chapter 6.1.).

#### 5.4 Structural observations

Few outcrops permitted direct observations of brittle deformation and provided information about the geometry of potential larger-scale structures. In the close vicinity of the Torony scarp, a sandpit (Fig. 3) exposes the Upper Miocene sequence including silt, cross-laminated sand and one organic-rich clay layer (Fig. 12, for location see Figs. 1 and 3). Several sets of faults and joints affected the poorly consolidated sediments (Figs. 12, 13). One set has NE-SW strike, and moderate, mainly south-eastern dip. Faults have normal separation from 10 to 80 cm, and few striations on fault planes preserve the dip-slip normal character. Some faults are combined with drag of the layers and show flattening in their upper section (Fig. 12). This indicates plastic state of sediment at the time of de-

formation. In other cases, the fault does not cut the uppermost clay layer which is just slightly bended. In one case, the organic-rich clay shows thicker section in the hanging wall than in the footwall, and thinning away from the fault (Fig. 12).

The other set of fractures is WNW-ESE trending and has steep dip (Fig. 13). These fractures have only cm-scale displacement, they are curved, and terminate against the south-east dipping faults. This abutting geometry suggests a genetic link between this and the former set, but in the lack of kinematic indices, the exact nature of this linkage remains questionable.

A third set of faults has NW-SE to NNW-SSE strike and gentle to moderate dip (30-60°). These faults displace the lower boundary of the clay layer but not the upper one, giving evidence for faulting during deposition of the clay layer. Finally, a single E-W striking left-lateral fault was observed which does not fit to one stress tensor with the previously mentioned normal faults.

Striated faults permitted the calculation of stress field of the deformation. When treated separately, the two striated sets give fault-perpendicular horizontal minimal stress axis, in NW-SE and NE-SW direction and excellent fit of faults to the stress tensor. Calculation of stress tensor for all faults resulted in an acceptable fit of all faults with the following observations for the misfit criteria. Average misfit angles (between the observed and calculated striae, A on Fig. 13) are smaller than 23° for all 25 faults. However, when considering the size of shear vector acting on the plane, the number of misfitting faults increased to four (criteria Rup, Angelier, 1990, R on Fig. 13). This means that although faults and striations are oriented in the direction of the resolved shear stress acting on fault planes, the value of the shear vector could be small. Slip could possibly happen because the frictional coefficient was low in the water-saturated clay layer, and even a low stress level and consequently low shear vector was enough to induce deformation.

However, the ratio  $\phi = \sigma_1 - \sigma_2 / \sigma_2 - \sigma_3$  (Ph on Fig. 13) is almost zero, so the direction of extension ( $\sigma_1$ ) is poorly constrained

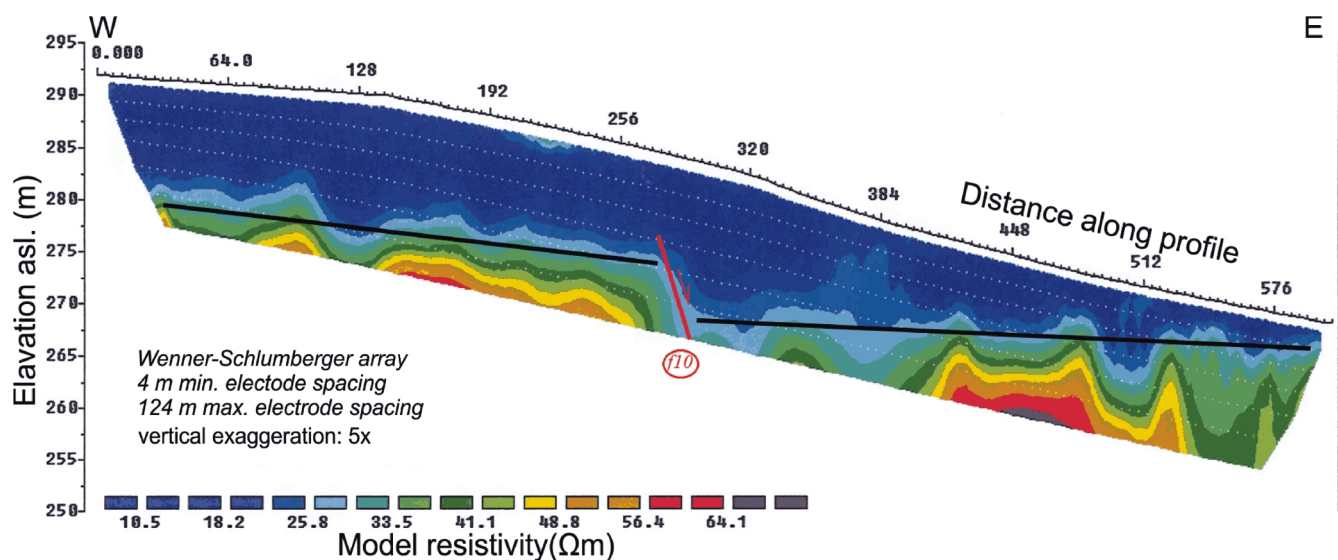


Figure 9: Result of 2D resistivity tomography. Note fault indicated by stepped form of resistivity values. For location see Fig. 3.

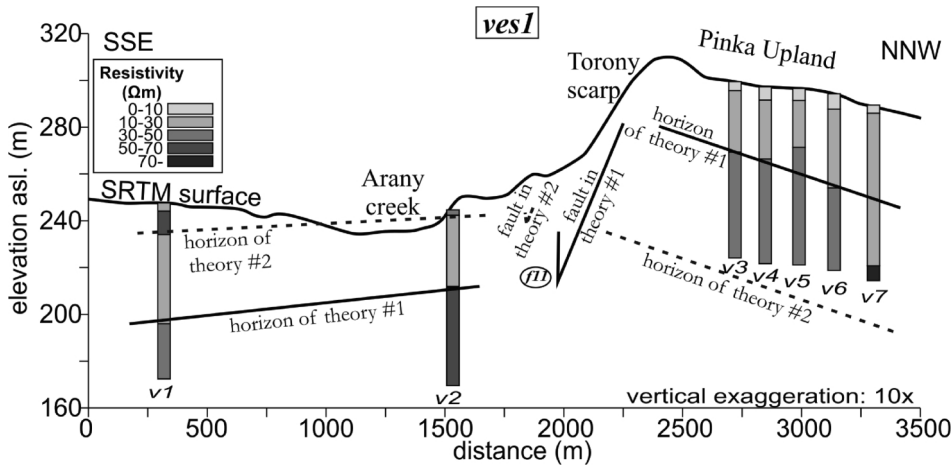


Figure 10: Section profiles using VES results (ves1). For location see Fig. 3.

and can be exchanged with  $\sigma_2$  axis. This bidirectional extension is in agreement with low-level stress deduced from misfit criteria and could be typical for the deformation of the Upper Miocene sediments. Sub-perpendicular fracture sets were described in several times elsewhere, e.g.e orthogonal sedimentary dykes (Winterer et al., 1991), sub-perpendicular faults in volcanic areas (Acocella and Funicello, 2006), cross faults on the Mars (Wilkins and Schulz, 2003) or the development of orthogonal fault system due to frequent permutation of stress axes  $\sigma_2$  and  $\sigma_3$  (Angelier and Bergerat, 1983).

Kinematic analysis and stress axis estimation was carried out in two other sites. In Bozsok site (Fig. 1) the Upper Miocene sandstone was deformed by joints with two directions: NNW–SSE and NNE–SSW. These two sets could have formed in two separate deformation episodes, with slightly varying extensional directions (ENE–WSW and ESE–WNW, respectively). Alternatively, the two sets of joints represent a 3D deformation field, due to ~E–W extension, as described by Reches (1978). In any case, these joints predates the tilting of layers, thus represent a relatively early deformation event(s).

One site (Felsőcsatár) was a greenschist quarry in the Penninic basement (Fig. 1), which underwent cooling from greenschist facies metamorphism in the Miocene (Dunkl and Demény,

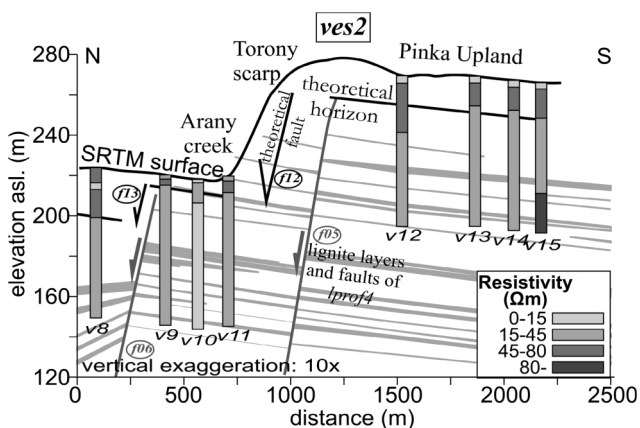


Figure 11: Section profiles using VES results (ves2) with layers and faults of lprof4. For location see Fig. 3.

1997, Cao et al., 2013), so brittle faults can not be older than Miocene in age. The observed two stress states could be connected with the regional structural evolution of the Pannonian Basin (Fodor et al., 1999). The first deformation step involves NNW–SSE trending normal faults with NE–SW trending sinistral faults (Fig. 13). Specifically, the estimated ENE–WSW extension direction is very similar to that one inferred for core complex exhumation of the Penninic rocks within the Rechnitz win-

dows (Tari, 1994, 1996). Thus, these structures could form during the syn-rift phase of the Pannonian Basin (Fodor et al., 1999), in the late Early to Middle Miocene. The second phase comprises oblique normal faults, trending NNW–SSE and NE–SW. Overprinting relationship between striations indicates that the second phase was the ESE–WNW extension; this direction is close to what we deduced from Upper Miocene sites.

The three analysed sites show certain similarities and differences. In all cases, the deformation was extensional, the direction of extension could vary between ENE–WSW to SE–NW. We do not know if this variation means spatial inhomogeneity within the deformation field or reflect several faulting episodes during the Late Miocene to recent time span. It is to note that Ratschbacher et al. (1990) noted similar extension in the Penninic rocks of the Rechnitz windows. They dated this event as being younger than NW–SE compression of Miocene age, but could not give precise age.

## 6. Discussion

### 6.1. Correlation of fault indications, 3D model of fault network

In this chapter we discuss the correlation of fault indications, the potential displacement of the faults and fault-related deformations. The results are shown on map and on a simplified 3D view (Figs. 14, 15). The westernmost *f03* and *f08* fault indications can be correlated to form *F1* fault (Fig. 14). This fault runs parallel to NW–SE directed reach of the Arany creek. Indication *f02* can belongs to an independent *F2* fault or could be, alternatively, part of *F1* if one assumes a strong curve of *F1* fault east from indication *f08*.

Further to east, we correlate *f01* fault of *lprof2* section with *f04* fault of *lprof3* profile (Fig. 14). Although less well constrained, the *ves1* profile crosses this *F3* fault at fault indication *f11*. This fault runs exactly at the foot of the Torony escarpment, along its NE–SW striking segment (Fig. 15). Parallel outcrop-scale faults are observed in the nearby sandpit (Fig. 12, 13) and described in historical lignite mines (Jaskó, 1947). Altogether, *F3* is the best constrained fault segment, where

the correspondence between the steep scarp and the faulted lignite beds are excellent. The displacement is less constrained and alternative solutions are discussed in the chapter 6.3.

The next *F4* fault is postulated on the basis of steep slope and analogue mesoscale faults in the outcrop (Fig. 13, 14). Fault *F5* is crossed by the MUEL profile at point *f10*; although

the direction of the fault is not constrained, we assume that the fault is expressed in the morphology as a small step and is parallel to the NE-trending main scarp segments. Fault *F6* has been postulated using the steep slope and because of similar morphological character as in case of *F2* and *F3*. Fault *F7* and *F8* are both controlled by sections based on boreholes

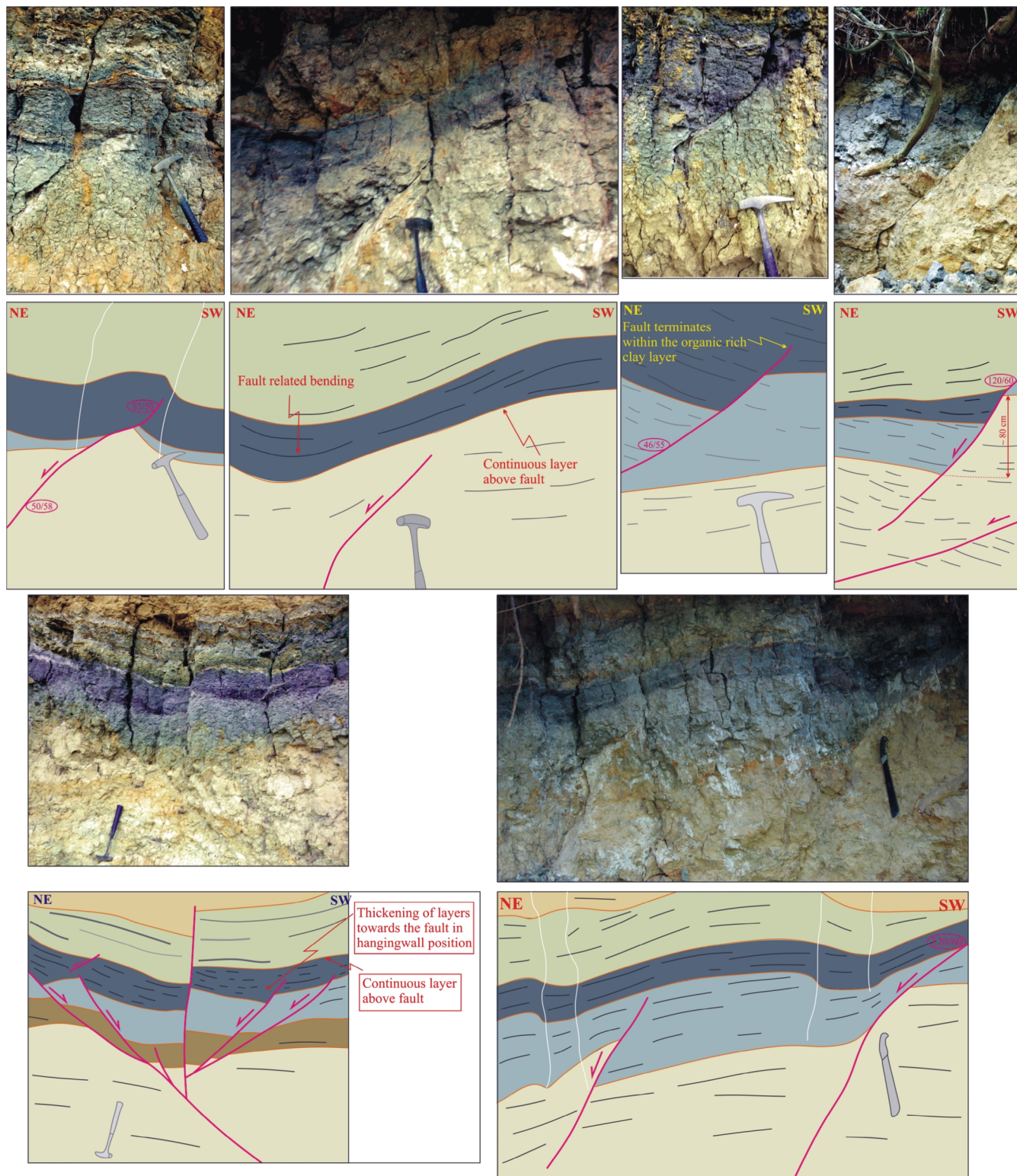


**Figure 12:** Field sketch with photos of outcrop-scale faults in a sandpit near Torony. Note syn-sedimentary thickening of lignite in hanging wall, and bending of layers above of faults.

and the *ves2* profile; the connected indications are *f05-f12* and *f06-f13*. This latter *F8* fault could be extended up to *lprof5* at *f09* (Fig. 14). Fault indications *f06* and *f09* correspond well with each other both in position and in throw value, however *f13* drops only 20 m (Fig. 11). Therefore the upper high resistivity strata of *v9-11* is considered as Pleistocene coarse grained sediment that also corresponds with borehole data (see *Sz-9* on Fig. 7). The strike of *F7* and *F8* faults is parallel to the NW–SE trending scarp segment. The position of *f12* in *ves2* correspond well with *f05* (Fig. 11), but their displacements are only comparable if we consider the rectangle-marked alternative correlation on Fig. 7.

## 6.2 Folds

Dip directions of lignite beds are changing in the sections. One systematic change is the flip of dip direction in ~N–S sections. While the southern part of the sections *lprof2*, 3, 4 and the entire *lprof1* show southerly dip, the northern portion of the sections more or less clearly suggest northerly dip. The

VES sections clearly support the southerly dip, while they are too short to demonstrate the northerly dipping northern portions. All these data are consistent with the presence of an updoming whose axis is trending ENE–WSW and located just north of the Torony scarp. The origin of this gentle fold is not clear; it can reflect upper crustal shortening, but could also have an origin as a drape fold above the subsurface continuation of basement rocks of the Eisenberg-Vas Hill ridge (see also Bereczki et al., 2013). In this latter case, the fold is just coincidentally closely located to the scarp.

On *lprof5*, the different position of lignite layers between borehole TO-45 than in TO-21 can also be solved by folding of the layers (Fig. 8). Here the discrete fault solution does not seem to be realistic, while the two inevitably postulated faults would not appear on other sections nor suggested by geophysical methods. The presence of a monocline can be logical, if one assumes that it is related to faulting along the *F3-F4* system, and represents a blind continuation of one of these structures to the north.

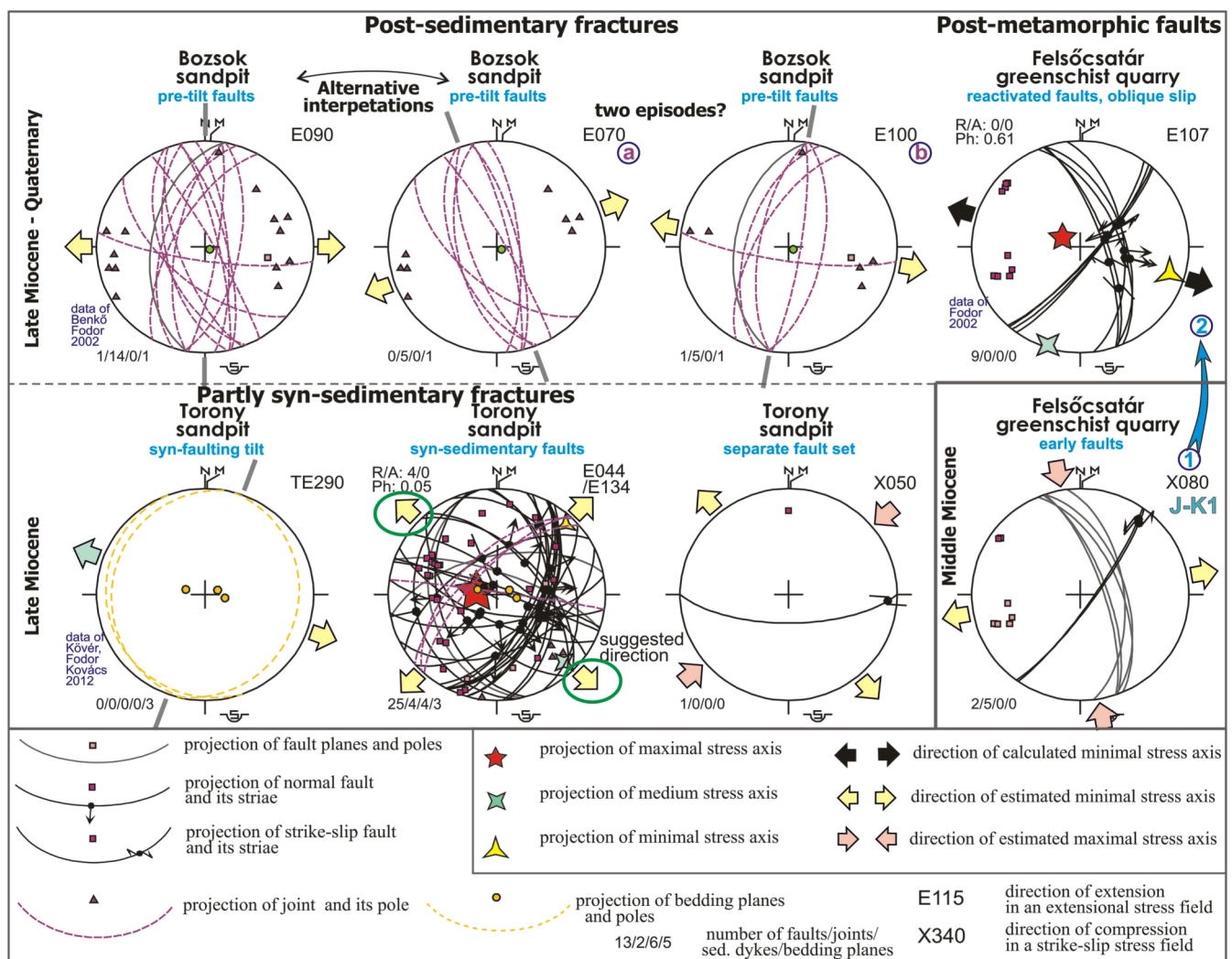


**Figure 13:** Stereographic representation of measured brittle structures in three sites near the study area. Site Felsőcsatár is a Jurassic-Cretaceous greenschist cooled into brittle regime the Miocene, while the two other sites are Late Miocene. Note extensional structures in the two latter sites and also in Felsőcsatár. Sign at upper left corner of stereograms marks the number of misfit faults: 0 if misfit angle (A) is smaller than 23°, and if criteria Rup (R) is smaller than 50. See Angelier (1990) for details.

Finally, we assume a gentle additional tilt of the lower layers of borehole TO-49. This is due to the larger thickness of intercalated sandy layers in borehole TO-49 with respect to Sz-9 (Fig. 7). This postulated tilt could be connected to the F8 fault and may represent a drag along the fault.

### 6.3 Displacement along fault: alternative solutions

Now we discuss that although the location of faults *F1*, *F3*, *F7* and *F8* is well constrained by various indices, the amount of total vertical displacement (throw plus bending, tilting) is not unequivocal. Borehole-based correlation of lignite beds and VES-based correlation of thicker sedimentary units issue different values for total displacement, ranging from 10 to 80 m.

We present one example, the geographically best constrained *F3* fault. Here we suggest two possible scenarios for correlation of lignite layers in the fault blocks. Concerning the *ves1* profile, the higher resistivity strata at lower position can be considered as the same as in the upland (Fig. 10, horizon of theory #1); in this case ~80 m vertical drop exists along the scarp (*f11*). According to the second option, the higher resistivity strata on Pinka Upland could be identified as the thin uppermost higher resistivity layer on the alluvial plane (Fig. 10, dashed line along the bottom of the strata). In this case, displacement is very small. Model #1 of the profile *ves1* (Fig. 10) corresponds with diamond-marked correlation of *lprof3*

(Fig. 6), while model #2 displaces layers with the same small amount as triangle-marked correlation on *lprof3*.

All such discrepancies may be due to different approaches; the borehole-based correlation considers individual beds while geophysical method images larger units. Both methods have pitfalls; the bed-to-bed correlation may fail to recognise lateral thickness variation and changing distance between lignite beds, thus issue false connections. The geophysically established boundaries between larger units depend on the modelled resistivity and the thickness, and can be shifted with a certain amount. Thus, we consider the problem of different displacement indices as due to the uncertainty of the applied methods; the exact determination of vertical deformation would need more detailed data. In any case, this uncertainty does not influence the presence and location of faults.

### 6.4 3D model and kinematics of the Torony faults

The NE–SW trending fault segments can be interpreted as arranged in an echelon geometry (Fig. 14, 15). The displacement along these segments could decrease toward their end points or transferred to the sub-perpendicular fault set. This is the case for *F3* fault (Fig. 6.) whose north-eastward projection does not appear on profile 5 (between TO-45 and -46 on Fig. 8). The *F6* fault west from Sé-3 borehole (Fig. 14) terminates before the profile 3 (Fig. 6). Here the strain could be trans-

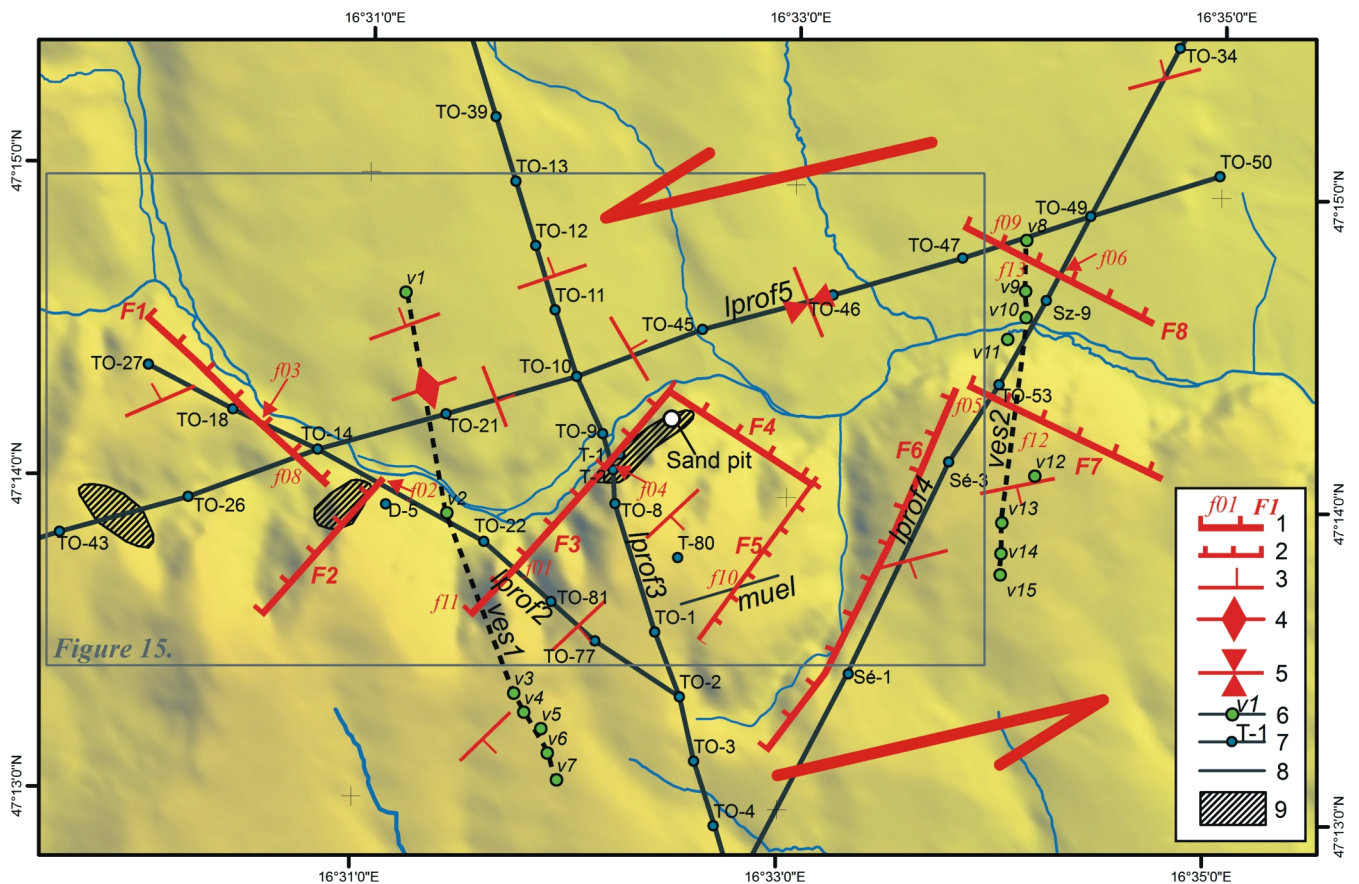


**Figure 14:** Overview map of the determined faults. Arrows indicate general sinistral movement. 1 – derived main fault with the name of identified segment (*f01*) and of the fault (*F1*); 2 – derived subsidiary fault; 3 – layers dip; 4 – anticlinal structure of layers; 5 – synclinal structure of layers; 6 – VES profile with measurement; 7 – section profile using boreholes; 8 – multielectrode profile of 2D resistivity tomography; 9 – lignite outcrop by Jaskó (1947)

ferred to the oppositely dipping *F5* fault imaged by the 'MUEL' profile (Fig. 9).

We interpret the NW–SE trending fault set as connecting fault splays between the main en echelon segments. Such connecting splays are typical for relay ramps, when the deforming parts between main faults are beached by secondary faults (Peacock and Sanderson, 1994). This relay ramp model could also explain the tilting (monoclonal bending) of layers in the northern block of the Torony fault system, e.g. postulated near boreholes TO-10 and -46.

The en echelon geometry of the NE–SW trending main faults, together with the connecting, sub-perpendicular sets form the complete fault system (Fig. 15). Applying the locally calculated SE–NW extension, or projecting ESE–WNW extension from nearby sites (Fig. 13), the fault system could have sinistral component of slip, in addition to the top-to-northwest displacement. The supposed buried sinistral or sinistral-normal fault may have ENE–WSW strike.

### 6.5 Maximum age of the deformation

The outcrop observation, that some faults do not cut the uppermost clay layers could be interpreted as sign of syn-depositional faulting or alternatively, accommodation of strain by ductile bending rather than rigid faulting (Fig. 12). However, the thickening of layers in the hanging wall, their wedge-shape geometry clearly demonstrates syn-depositional faulting with respect to the clay layer. These syn-sedimentary faults seem to indicate that deformation started during the Late Miocene sedimentation. Similar suggestion can be made on *lprof4* (Fig. 7); the thicker sand intercalations in the hanging wall block (TO-49) and the postulated tilt (drag fold) of the lower layers could indicate continuous slip during sedimentation. On the other hand, the deformation mostly post-dates the Late Miocene lignite layers. The age of lignite-bearing strata is poorly known. Better age constraints provide the underlying shelf-slope units, which prograded across this part of the Pannonian

Basin between 9.7 and 9 Ma (Magyar et al., 2007, 2013) or at 8.7 Ma (Lantos and Hámor, 1989). For the overlying units, Lantos and Hámor (1989) suggested 8.3 Ma as the age of the uppermost Miocene sediment based on the reverse magnetic polarity of Late Miocene sediment and paleontological investigations. Thus, the deformation of the Torony fault system could not start earlier than 8.7 Ma, as the syn-sedimentary part of the faulting. On the other hand, most of the slip occurred after 8.3 Ma.

### 6.6 Possible neotectonic interpretation of the fault system

Discussion on the possible youngest age of movement along the scarp implies data on the amount of displacement and all geomorphic process having acted around the scarp. In both the northern and southern block, formation of pediment surfaces represents an important Quaternary process which led to gently dipping surfaces. These surfaces were later incised by SSE-flowing small creeks. Our geomorphological analysis seems to suggest that at least some of the creeks used to flow to the south continuously above the present location of the Torony scarp before being captured by the eastward flowing lower Arany creek. Disruption of formerly continuous ~N–S valleys might have occurred due to fault-induced subsidence or, alternatively, erosional lowering of the northern block. In any case, the emerging morphological scarp diverted the Arany creek from its former course to fault-parallel (ENE–WSW) orientation.

The main question related to the possible youngest age of faulting is if the height of the scarp is the same and thus comparable to the vertical displacement of the lignite layers. The other question is if the hanging wall and footwall contain the same, albeit thin, post-lignite (Quaternary) sediments. As discussed in a previous chapter, the amount of displacement is not perfectly constrained. Considering borehole-based correlation, the throw of faults seem to be smaller than the height

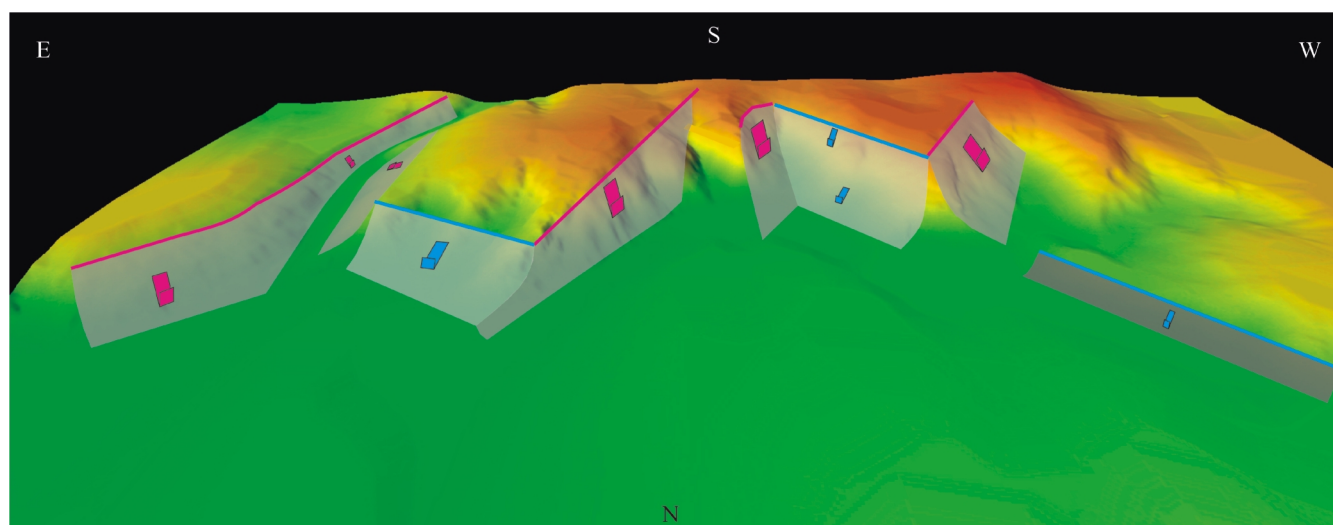


**Figure 15:** 3D model of the Torony fault system, projected onto the DEM of the area. Note en echelon fault segments controlling the main scarps and sub-perpendicular connected fault splays.

of the morphological step. In this case, the northern hanging wall block would suffer additional denudation, which does not occur in the elevated southern (footwall) block. This could increase the height difference between the two blocks. This scenario may find support in the fact, that (1) the southern block is less steeply incised by the N-S drainage than in the lower northern block (Fig. 2d,e), (2) although in both blocks the post-lignite (Quaternary) cover is similar in composition, (gravel, sand, and younger loess) the gravel is different in the two blocks. In the south, pebbles are coated with desert varnish or at least with iron-oxide-hydroxide film, while it is missing in the north. The southern gravel is more continuous and grain-supported, while gravel is sandier in the north. All these features may suggest the interpretation that the southern block has its original older gravel carpet, which might have formed as an extensive pediment carpet, while in the north the gravel is younger and has been redeposited from the older pediment cover and mixed with younger sand (Fig. 16A). The denudation of the northern block could happen by surface wash during the early(?) to middle Pleistocene. Incision of present-day small valleys into the former pediment surfaces could start only in late Middle Pleistocene, accepting numerical ages from the central Pannonian Basin (Thamó-Bozsó et al., 2010). In this scenario faulting would have started before the pediment formation, and could continue after it, in the Quaternary (Fig. 16A). However, differential erosion should have occurred, lowering more the northern block. In this case the

scarp-parallel updoming has to be present before pediment formation otherwise the pediment surface should have been slightly folded (Fig. 16A).

Accepting a larger displacement scenario for the scarp-related *F1, F3, F6-F8* faults, the height of slope would be similar to the total vertical deformation. In this case one can suppose that a formerly continuous landform (a pediment with cover sediments) was deformed by the Torony fault system (Fig. 16B). This would imply that the entire deformation post-dated the Quaternary pediment formation and its gravel carpet, which would have serious implication for neotectonic studies. In this case the fault scarp would only be connected to neotectonic deformation. This model would discard the observed Late Miocene syn-sedimentary deformation and does not explain the effect of the scarp-parallel updoming.

Presence of active mass movement processes and deep erosional gullies suggest that the slope is still unstable (despite the rich vegetation) and it was steeper than today; this may also be an indirect indication of fault-controlled slope development (Fig. 14) as described by several authors (e.g. Fubelli et al., 2009). Scheingross et al. (2013) indicated increased amount of earth flows along the creeping segment of the San Andreas Fault. In our study area, we cannot infer recent fault activity because the lack of comparative observation of landslides and earth flows at other slopes of the wider area.

Although we cannot exclude a completely neotectonic origin, we favour a complex history, when faulting started in the

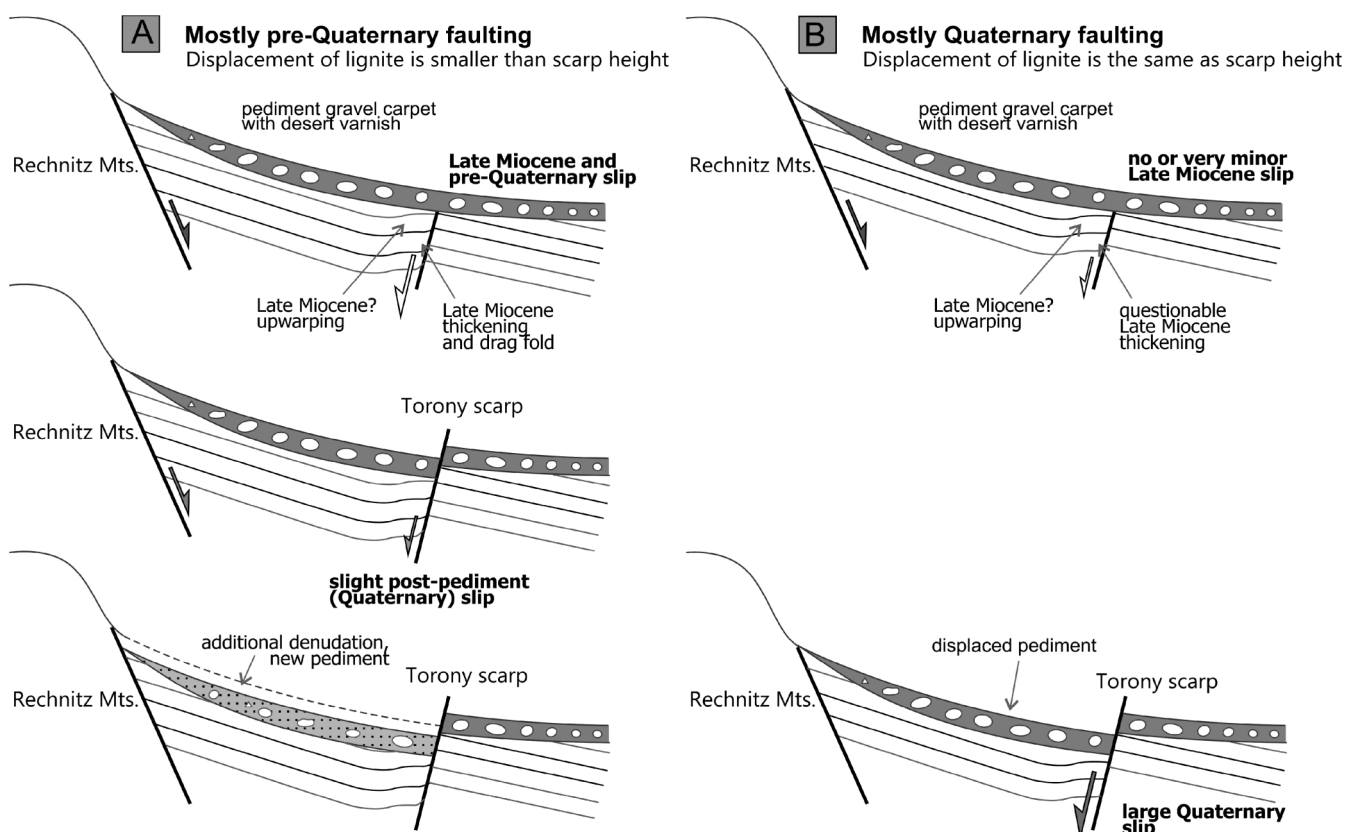


**Figure 16:** Conceptual model for the age and displacement along the Torony scarp. Note changing displacement in different time slices. See discussion in the text.

Late Miocene, continued in the Quaternary before and/or after the pediment formation.

### 6.7 Tectonic origin of the drainage anomaly

All of the previously discussed surface and subsurface structural data are in agreement with the assumptions based on the DEM: the Torony segment of the Arany creek is controlled by a fault system. It is composed of two sets: one trending NE–SW and one (W)NW–(E)SE (Fig. 14). Upper Miocene layers are deformed mainly along the scarp and are only slightly disturbed farther away, as demonstrated by the *lprof1* (Fig. 4), and the undisturbed southern segment of *lprof3* (Fig. 6), and minor faults at the northern end of *lprof4* (Fig. 7). Thus our analysis verified without doubt the localised deformation and its control on the landforms. In outcrop scale, the observed fault pattern also mimics the directions of the slope segments which occur in the close vicinity, which give further credit for fault-controlled slope development.

### 6.8 Remarks on method applicability

The morphology of the Arany creek valley strongly suggests a tectonic control at a glance. However, the poor outcrop conditions prohibit direct demonstration of faults or folds controlling the steep slopes of the Torony scarp. In case of layers undisturbed by subsequent deformation (as under Pinka Upland, see *lprof1* in Fig. 4 and *lprof3* in Fig. 6 apart from the scarp), correlation of lignite horizons between boreholes is relatively unambiguous.

Here we note some remarks on the combination of the applied methods that may have more general methodological message. Correlating strata appearing in borehole data and 1D VES measurement were applicable only with complementary measurements and observations.

The highly variable structure of lignite horizons are difficult to interpret without the pre-existing structural observations in lignite mines, preliminary geomorphic analyses of steep scarps and the analyses of the outcrop-scale structures. For geoelectrical methods both array types have to be chosen to achieve deep enough penetration. Hilly surface of the study area, the studied steep scarps, tilted and disturbed layering altogether suggested the choice of deeper penetration for VES measurements and also the usage of the Wenner-Schlumberger array type of multielectrode measuring. MUEL proved to be a successful method in mapping subsidiary fault segment. In that case the scarp is less steep and less high as the main fault, therefore shallower penetration was enough to detect faulted layers. VES measurements were able to separate different resistivity sediment units, therefore quasi-horizons could be correlated using additional information from boreholes and structural observations. According to Štěpančíková et al. (2011) the applied methods could be distinguished to different scales: borehole data provided regional information about general tilting of the layers and locations of disturbances. Using VES, data distribution could be densified, while MUEL could be applied in case of smaller deformations.

Structural observations were useful to determine the fault-slip data locally, that could be projected to the neighbourhood.

An important issue of our work is that the combination of diverse methods is useful, sometimes inevitable for checking the potential structural control on landform and landscape evolution, like it was suggested by earlier works (e.g. Marple and Talwani, 2000; Caputo et al., 2003; Alasset and Meghraoui, 2005; Fodor et al., 2005).

### 6.9 Regional context of the Torony fault

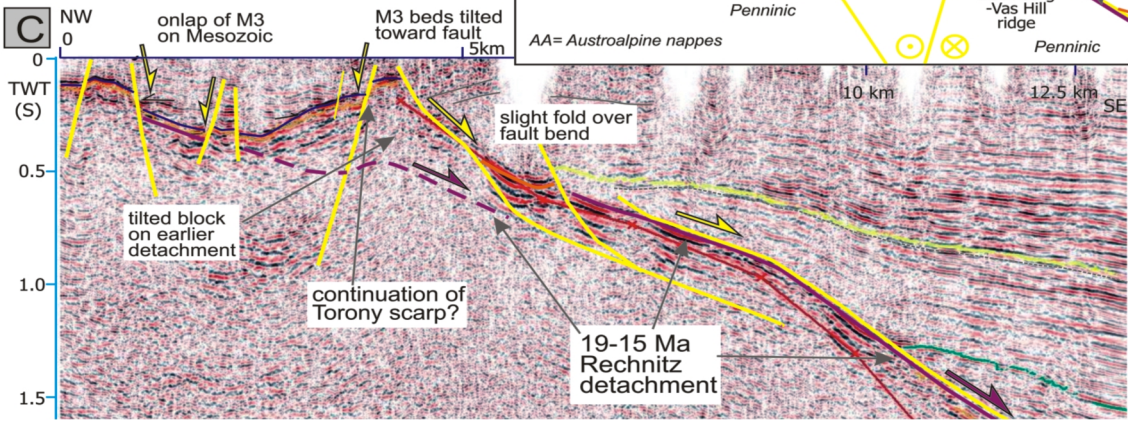
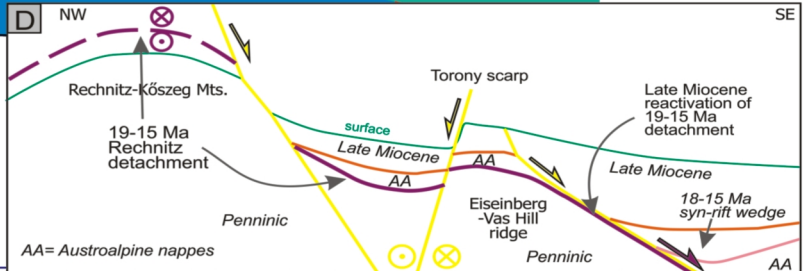
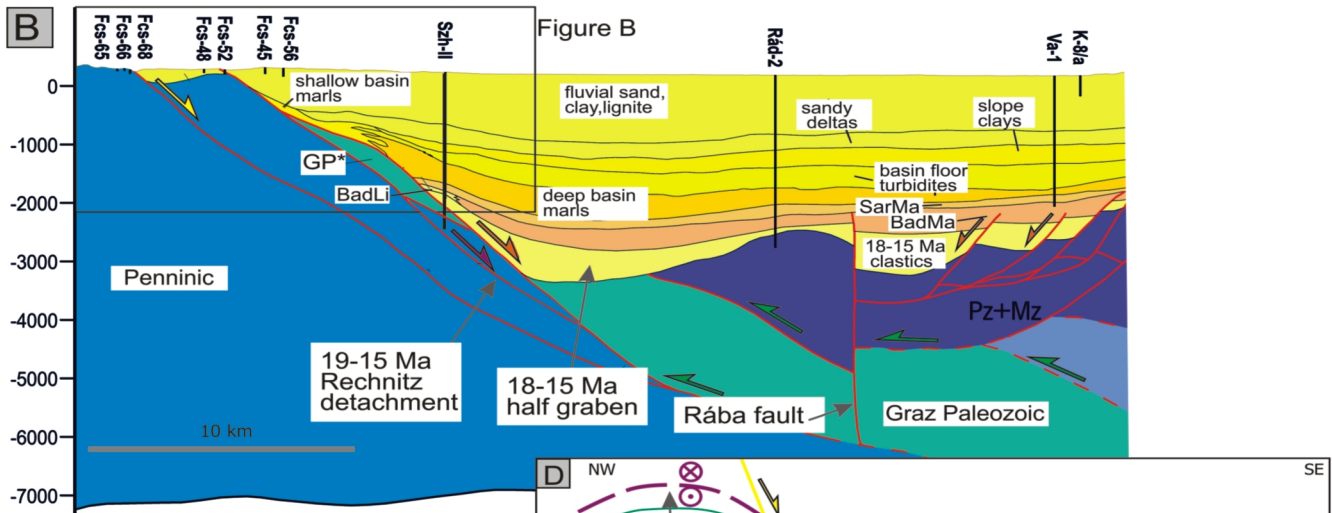
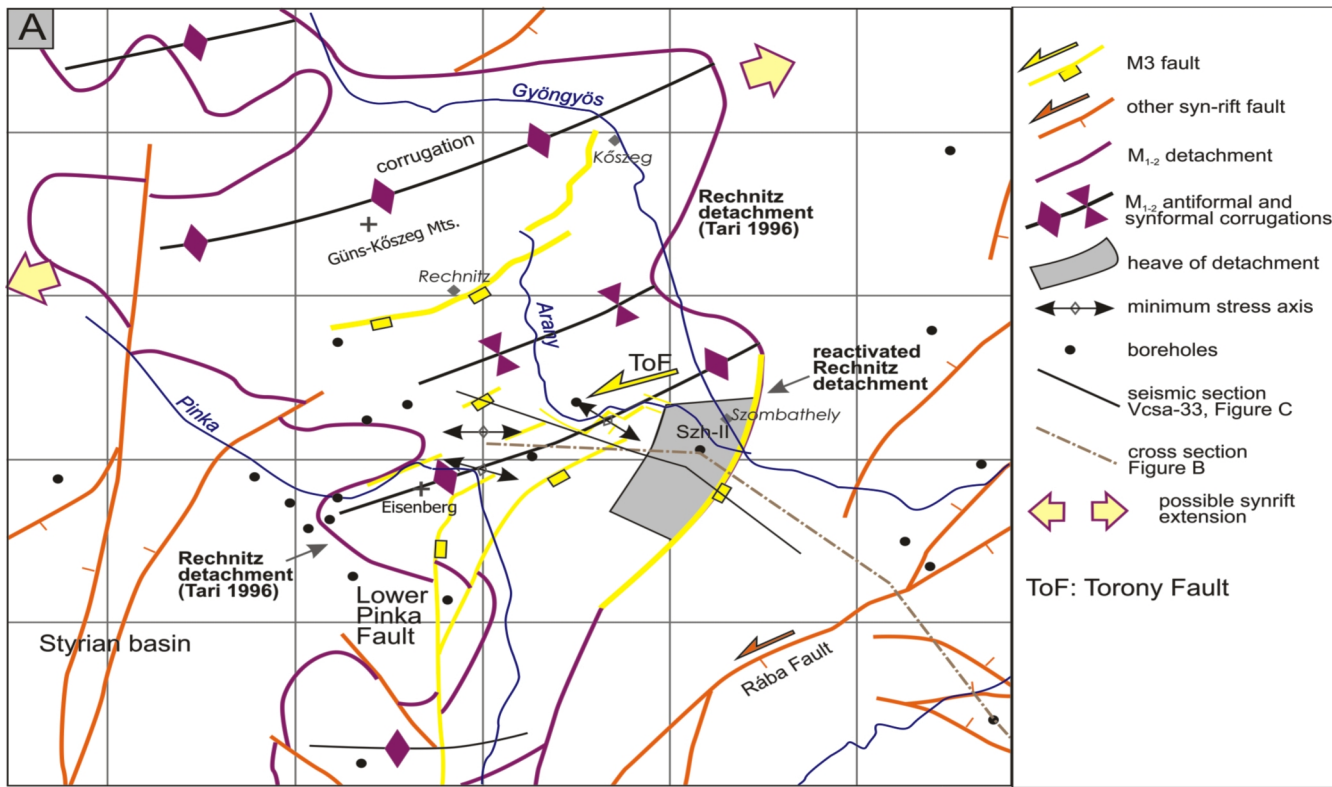
The demonstration of a structural origin of the Torony scarp is an important result of the combined methodology. Further on, the detection of the Torony fault, the minimum age and style of the motion are important additional information that may help to understand neighbouring structures, such as the Eisenberg–Vas Hill and Rechnitz–Kőszeg Mts.

The Rechnitz–Kőszeg Mts. have a clear ENE–WSW strike. The Eisenberg–Vas Hill is small, but equally elongated in the same direction (Fig. 17A). The eastward extension of Penninic rocks below Miocene sediments was only roughly depicted by Kilyényi et al. (1991), whereas in the map of Haas et al. (2010) it was even not shown. A new data compilation of Fodor et al. (2013b) was not detailed enough to show the basement morphology. On the other hand, new measurements of Bereczki et al. (2013) demonstrated that the Eisenberg–Vas Hill continues toward ENE and Penninic rocks form a subsurface ridge (Eisenberg ridge) in the pre-Neogene level.

Tari (1996) interpreted the elongation of the Rechnitz–Kőszeg Mts. and the Bernstein window as reflecting large-scale corrugations which could develop during the late Early to Mid-Miocene tectonic exhumation of the Penninic units. This exhumation occurred along a low-angle detachment, the Rechnitz detachment, which forms the boundary between the lower Penninic and overlying Austroalpine units (Ratschbacher et al., 1990, Tari, 1996). This deformation probably occurred due to ENE–WSW extension, parallel to the corrugations. Alternatively, the elongated corrugate structures could be formed due to noticeable NNW–SSE shortening, contemporaneous to the ENE directed extension; a similar scenario was postulated along core complexes in the western USA (Singleton, 2013). This scenario was postulated by Ratschbacher et al. (1990) and Cao et al. (2013). Our fault-slip data from the Penninic rocks are in agreement with NNW–SSE shortening (Fig. 13).

Although both scenarios are viable, our observations suggest that the present-day geometry of Penninic basement

**Figure 17:** Relationship of syn-rift and post-rift faults near the Rechnitz–Kőszeg Mts. A) Sketch map for Miocene structures near the study area, indicating the boundary (detachment fault) of the Penninic unit (Flügel, 1988, Fodor et al., 2013b). Faults of the Torony scarp are exaggerated. B) Geological cross section, partly following the seismic section line (Fodor et al., 2013b, modified). Pz+Mz: Permo-Mesozoic of the Transdanubian Range unit. Frame shows the location of seismic line. SzH-II: Szombathely-II borehole. C) Seismic section across the Eisenberg ridge (after Tari et al., 1992). D) Sketch showing the possible reactivation and cut of the syn-rift detachment by Late Miocene faults.



high is at least partly connected to Late Miocene and younger deformation. Along the southern boundary of the Rechnitz window, the steep slope can hardly be an inherited southern limb of the syn-rift antiformal corrugation without post-detachment deformation. We suggest that Late Miocene or younger faulting increased the probably pre-existing structural relief (Fig. 17A). Because these faults are structurally below the upper Penninic detachment, they are independent from it and are not its reactivation. On the other hand, the Late Miocene throw could be smaller than the maximum 1000-1500 m structural relief and contributed only to a minor extent to the uplift of the Penninic rocks.

Our detailed study offers another argument for the Late Miocene or younger amplification of ENE trending corrugations. The Torony fault system is parallel to the Eisenberg basement ridge (corrugation) and is located close to the hinge zone (Fig. 17A). The Torony fault can continue westward according to the seismic line *Vcsa-33* presenting deformed Upper Miocene sediments (Tari et al. 1992, Fodor et al. 2013b). Here in Upper Miocene sediments a syncline developed which is faulted at its limbs. Further west, the northern slope of the Eisenberg–Vas Hill can be controlled by ENE trending fault. These faults seem to cut across the syn-rift low-angle detachment seen on the seismic line (Fig. 17C).

The southern side of the Eisenberg ridge is also very sharp at the outcropping part and a NE trending fault can be postulated. Starting from the surface boundary of the ENE trending Eisenberg Penninic ridge, a N–S striking important fault splays off from the southern side of the ridge and runs along the Austrian-Hungarian border (Fig. 17A). This Lower Pinka fault borders the South Burgenland swell on the east; it was detected by Nebert (1979), mapped by Flügel (1988), recently Fodor et al. (2013b) and measured by geophysical methods (Bereczki et al., 2013). This fault clearly displaces the Penninic-Austroalpine boundary (the syn-rift Rechnitz detachment), as shown on the map of Flügel (1988), Tari (1996) and Fodor et al. (2013b).

Southeast from the Eisenberg ridge, the seismic line depicts a major fault zone which is a moderately to gently dipping normal fault (Tari et al., 1992, Fodor et al., 2013b) reached by borehole Szombathely-II (Fig. 17B, C). This major fault zone is part of the Rechnitz detachment (Tari, 1996) and forms the eastern boundary of the Penninic rocks. In its hanging wall, a large asymmetric half graben is the southern extension of the Danube basin (Fodor et al., 2013a).

This system of combined N–S to ENE–WSW trending ridges and boundary faults can be interpreted in terms of kinematics based on our scattered fault-slip data. They seem to indicate a sinistral or sinistral-normal kinematics along the ENE trending structures like the northern and southern boundary of the Eisenberg ridge, while the N–S to NNE–SSW striking structures could have pure dip-slip normal character.

The deformation of the Torony fault is clearly younger than the classical main phase of rifting of the Pannonian Basin, referred to as syn-rift faulting, which occurred in the late Early

to Middle Miocene (ca. 19-11 Ma, Horváth and Royden, 1981, Fodor et al., 1999) and thus younger than extensional exhumation by low-angle detachment faults of Karpatian age (Tari, 1996). At the seismic profile the Late Miocene sediments clearly abut (onlap) against the southern Eisenberg ridge (Fig. 17B, C), while several major sedimentary units are missing from the footwall block. This geometry suggests Late Miocene slip along this segment of the Rechnitz detachment fault. On the other hand, the fault was active already in the late Early to Middle Miocene, because the correlative sediments form a half graben (Fig. 17B) and are missing from the Eisenberg ridge. In this case, the Early to Mid-Miocene syn-rift detachment fault was reactivated by a later deformation, namely during and after the Late Miocene sedimentation.

These observations suggest that the Late Miocene (and younger) deformation partly reactivated, partly displaced the generally low to moderately dipping syn-rift structures (Fig. 17D). The explanation for the presence of both reactivated and cut detachment fault segments could be in their present-day depth and dip. Those detachment segments which are deep enough and have moderate dip could be reactivated during Late Miocene, like along the eastern margin of the Eisenberg Ridge, near Szombathely-II borehole (Fig. 17B, C, D). The possibility of reactivation lies in the fact, that syn-rift corrugations coincidentally have planes in directions which could, albeit obliquely, slip in the Late Miocene stress field, too. Those detachment segments which are close to the surface, and/or are very gently dipping, were cut by newly formed post-rift (Late Miocene) faults; this is the case on the southern Rechnitz window, at the Lower Pinka Fault and along the studied Torony Fault (Fig. 17A, D). It is not excluded that these post-rift faults would, at depth, merge syn-rift detachments located within or below the Penninic rocks.

The Torony fault and others around the Eisenberg Hill and Rechnitz window are new elements of the increasing number of Late Miocene (post-rift) faults which were presently summarised by Fodor et al. (2013a). Late Miocene deformation in general is more important than previously considered by the classical subdivision into syn-rift/post-rift phase (Royden and Horváth, 1988). Our study thus contributes to future reassessment of the classification of deformation phases in the Pannonian Basin.

## 7. Conclusions

This paper emphasizes the advantage and necessity of simultaneous usage of geophysical measurements, field observations, morphological analyses and borehole data to demonstrate the fault control on the asymmetric valley segment of the Arany creek, western Hungary. Borehole data combined with geophysical measurements constrained the location of possible fault segments which all are closely located to steep slopes. The combined data sets permitted the determination of the dip of Late Miocene lignite-bearing strata in certain fault blocks. The Torony fault system is composed of an echelon NE–SW segments and sub-perpendicular connecting splays

which resemble to breaching faults of relay ramps.

The en echelon faults could be part of a sinistral or oblique-slip shear zone, which occur between the Rechnitz and Eisenberg windows of the Penninic unit. The data suggest that tectonic exhumation of the Penninic unit continued after the main Early to Middle Miocene phase, although the fault geometry changed from low-angle to steep faults. The Torony fault is part of a system of Late Miocene or younger faults which partly reactivated, partly dissected the earlier syn-rift faults of the western Pannonian Basin. Our study shows that the Late Miocene basin fill of the Pannonian Basin was deformed considerably.

The described fault zone could be initiated in the Late Miocene (Pannonian) after 8.7 Ma and was active afterwards. The neotectonic role of the fault has not been clarified unequivocally; in one scenario faulting could predate Quaternary pediment formation, while in others it can be completely younger than this surface.

### Acknowledgements

Geophysical measurements were supported by the grant of OTKA NK 83400, field work of Fodor and Kövér was supported by the grant OTKA K 81530. The present research is partly realized in the frames of TÁMOP 4.2.4.A/2-11-1-2012-0001 high priority "National Excellence Program - Elaborating and Operating an Inland Student and Researcher Personal Support System convergence program" project's scholarship support, using Hungarian state and European Union funds and co-finances from the European Social Fund. The work of Telbisz T. has been supported by the János Bolyai Scholarship of the Hungarian Academy of Sciences.

### References

- Acocella, V. and Funicello, R., 2006. Transverse systems along the extensional Tyrrhenian margin of central Italy and their influence on volcanism. *Tectonics*, 25/2, TC2003. <http://dx.doi.org/10.1029/2005TC001845>
- Alasset, P.-J. and Meghraoui, M., 2005. Active faulting in the western Pyrénées (France). Paleoseismic evidence for late Holocene ruptures. *Tectonophysics*, 409, 39–54. <http://dx.doi.org/10.1016/j.tecto.2005.08.019>
- Anderson, E. M. 1951. The dynamics of faulting and dyke formation with application to Britain. Oliver and Boyd, Edinburgh 206 pp.
- Angelier, J., 1984. Tectonic analysis of fault slip data sets. *J. Geophysical Research* 89/B7, 5835–5848.
- Angelier, J., 1990. Inversion of field data in fault tectonics to obtain the regional stress - III. A new rapid direct inversion method by analytical means. *Geophysical J. International*, 103, 363–373.
- Angelier, J., and Bergerat, F., 1983. Systemes de contrainte et extension intracontinentale. *Bulletin Centres Rech. Exploration-Production Elf-Aquitaine*, 7/1, 137–147.
- Balla, Z., 1993. A kistápai gyengén metamorf képződmények tektonikai minősítéséről [Tectonic ranking of low level metamorphic formations in Little Hungarian Basin]. *Földtani Közöny*, 123/4, 465–500 (in Hungarian).
- Berczki, L.; Gärtner, D.; Kemény, M.; Péntek, A.; Kovács, G.; Timár, G.; Molnár, G. and Székely, B., 2013. Where do the Alps' foothills end? The depths of the Pre-Cenozoic basement in the foreground of Vas-hegy – Alpokalja, Western Hungary. *Geographica Napocensis*, 7/2, 33–42.
- Berry, M. E., Knuepfer, P. and McFadden, L. (Eds.), 1990. Soil catena development on fault scarps of different ages, eastern escarpment of the Sierra Nevada, California. *Geomorphology, Soils and Landscape Evolution*, 3, 333–350.
- Bödöcs, A., Kovács, G. and Anderkó, K., 2014. The impact of the roman agriculture on the territory of Savaria. *Dissertationes Archaeologica*, 3/2, 321–332.
- Cao, S., Neubauer, F., Bernroider, M., Liu, J. and Genser, J., 2013. Structures, microfabrics and textures of the Cordilleran-type Rechnitz metamorphic core complex, Eastern Alps. *Tectonophysics*, 608, 1201–1225. <http://dx.doi.org/10.1016/j.tecto.2013.06.025>
- Caputo, R.; Piscitelli, S.; Oliveto, A.; Rizzo, E. and Lapenna, V., 2003. The use of electrical resistivity tomographies in active tectonics: examples from the Tyrnavos Basin, Greece. *Journal of Geodynamics*, 36, 19–35. [http://dx.doi.org/10.1016/S0264-3707\(03\)00036-X](http://dx.doi.org/10.1016/S0264-3707(03)00036-X)
- Colella, A.; Lapenna, V. and Rizzo, E., 2004. High-resolution imaging of the High Agri Valley Basin (Southern Italy) with electrical resistivity tomography. *Tectonophysics*, 386, 29–40. <http://dx.doi.org/10.1016/j.tecto.2004.03.017>
- Dill, H., Hahne, K. and Shaqour, F., 2012. Anatomy of landslides along the Dead Sea Transform Fault System in NW Jordan. *Geomorphology*, 141–142, 134–149. <http://dx.doi.org/10.1016/j.geomorph.2011.12.031>
- Dombrádi, E., 2012. Deformation of the Pannonian lithosphere and related tectonic topography: a depth-to-surface analysis. *Utrecht studies in earth sciences*, 19, 1–176.
- Dunkl, I. and Demény, A., 1997. Exhumation of the Rechnitz Window at the border of Eastern Alps and Pannonian basin during Neogene extension. *Tectonophysics*, 272, 197–211.
- Eicher, H., 1994. A Kelet-Stájer-Alpok előhegységének geomorfológiai sajátosságai [Peculiarity in Quaternary geomorphology of the East Styrian Alpine Foreland]. *Földrajzi Értesítő*, 43, 29–39 (in Hungarian with English abstract).
- Fekete, Zs., 2011. A Pinka-fennsík kavicstakarójának helyzete és morfológiája. BSc Thesis, Dept. of Physical Geography, Eötvös Loránd University, Budapest, 38 pp. (in Hungarian)
- Fekete, Zs. and Kovács, G., 2012. Reconstruction of gravel coverage on an Eastern Alps foothill. *Geophysical Research Abstracts*, 14, #857.
- Fellner, D. and Hermann, P., 1993. Bericht 1992 über geologische Aufnahmen von Massenbewegungen auf Blatt 167 Güssing. *Geologische Bundesanstalt*, p. 653.
- Flügel, H. W., 1988. Steirisches Becken – Südburgenlandische Schwelle. *Geologische Karte des prätertiären Untergrundes*,

- 1:200. 000 Geologische Bundesanstalt Wien.
- Fodor, L., Csontos, L., Bada, G., Györfi, I. and Benkovics, L., 1999. Tertiary tectonic evolution of the Pannonian basin system and neighbouring orogens: a new synthesis of paleostress data. In: B. Durand, L. Jolivet, F. Horváth and M. Séranne (eds.), *The Mediterranean Basins: Tertiary extension within the Alpine Orogen*. Geological Society London Special Publications, 156, pp. 295–334.
- Fodor, L., Bada, G., Csillag, G., Horváth, E., Ruszkiczay-Rüdiger, Z., Palotás, K., Síkhegyi, F., Timár, G., Cloetingh, S. and Horváth, F., 2005. An outline of neotectonic structures and morphotectonics of the western and central Pannonian Basin. *Tectonophysics*, 410, 15–41. <http://dx.doi.org/10.1016/j.tecto.2005.06.008>
- Fodor, L., Uhrin, A., Palotás, K., Selmeczi, I., Tóthné Makk, Á., Riznar, I., Trajanova, M., Rifelj, H., Jelen, B., Budai, T., Muráti, J., Koroknai, B., Mozetič, S., Nádor, A. and Lapanje, A., 2013a. Geological and structural model of the Mura–Zala Basin and its rims as a basis for hydrogeological analysis. *Magyar Állami Földtani Intézet Évi Jelentése*, 47–91 (in Hungarian with English abstract).
- Fodor, L.I., Sztanó, O., Magyar, I., Törő, B., Uhrin, A., Várkonyi, A., Csillag, G., Kövér, Sz., Lantos, Z. and Tőkés, L., 2013b. Late Miocene depositional units and syn-sedimentary deformation in the western Pannonian basin, Hungary. 11<sup>th</sup> Workshop on Alpine Geological Studies and 7th European Symposium on Fossil Algae. In: R. Schuster (ed.), *Abstracts and Field Guides*. Schladming, 8–14th September 2013. *Berichte der Geologischen Bundesanstalt*, 99, 33–34.
- Fubelli, G., Gori, S., Falcucci, E., Galadini, F. and Messina, P., 2009. Geomorphic signatures of recent normal fault activity versus geological evidence of inactivity: Case studies from the central Apennines (Italy). *Tectonophysics*, 476, 252–268. <http://dx.doi.org/10.1016/j.tecto.2008.10.026>
- Gallousi, C. and Koukouvelas, I. K., 2007. Quantifying geomorphic evolution of earthquake-triggered landslides and their relation to active normal faults. An example from the Gulf of Corinth, Greece. *Tectonophysics*, 440, 85–104. <http://dx.doi.org/10.1016/j.tecto.2007.02.009>
- Goswami, R., Mitchell, N. C. and Brocklehurst, S. H., 2011. Distribution and causes of landslides in the eastern Peloritani of NE Sicily and western Aspromonte of SW Calabria, Italy. *Geomorphology*, 132, 111–122. <http://dx.doi.org/10.1016/j.geomorph.2011.04.036>
- Haas, J., Budai, T., Csontos, L., Fodor, L. and Konrád, G., 2010. Pre-Cenozoic geological map of Hungary 1:500000. Geological Institute of Hungary. Horváth, F., and Royden, L., 1981. Mechanism for the Formation of the Intra-Carpathian Basins: a Review. *Earth Evolution Sciences*, 1/3–4, 307–316.
- Hermann, P., 1990. Bericht 1989 über geologische Aufnahmen auf den Blättern 167 Güssing und 168 Eberau. *Jahrbuch der Geologischen Bundesanstalt* 133/3, p. 479.
- Herrmann, P., Fellner, D. and Schönlaub, H. P., 1993. Geologische Karte der Republik Österreich, 167 Güssing, 1:50 000. Geologische Bundesanstalt.
- Horváth, F. and L. Royden, 1981. Mechanism for the formation of the intra-Carpathian basins: a review. *Earth Evolution Science* 1, 307–316.
- Horváth, F. and Cloetingh, S., 1996. Stress-induced late-stage subsidence anomalies in the Pannonian Basin. *Tectonophysics*, 266, 287–300.
- Jaskó, S., 1947. Szombathely és környékének geológiája különös tekintettel a lignitelfordulásokra. Magyar Állami Földtani Intézet (in Hungarian).
- Juhász, E., Pillips, P., Müller, P., Ricketts, B., Tóth-Makk, Á., Lantos, M. and Ó-Kovács, L., 1999. Late Neogene sedimentary facies and sequence in the Pannonian Basin, Hungary. In: B. Durand, L. Jolivet, F. Horváth, M. Séranne (eds.), *The Mediterranean Basins: Tertiary extension within the Alpine Orogen*. Geological Society Special Publications, 156, 335–356.
- Kilényi, É., Kröll, A., Obernauer, D., Sefara, J., Steinhauser, P., Szabó, Z. and Wessely, G., 1991. Pre-Tertiary basement contour map of the Carpathian Basin beneath Austria, Czechoslovakia and Hungary. *Geophysical Transactions*, 36, 15–37.
- Kisházi, P. and Ivancsics, J., 1981. A Sopron környéki ottnangien és karpatien képződmények összefoglaló ismertetése [Overall review of Ottnangian and Carpatian formations around Sopron]. Unpublished manuscript, Hungarian Geological Institute.
- Koller, F. and Pahr, A. 1980: The Penninic ophiolites on the eastern edge of the eastern Alps. *Ofioliti* 5, 65–72.
- Kovács, G., Székely, B. and Papp, S., 2008. Observations of the surface evolution of Pinka-plain: mass movements and neotectonics. In: K. K. Hans and K. Raimund (eds.), *Proceedings of the Junior Scientist Conference*, pp. 309–310.
- Kovács, G. and Telbisz, T. 2013. Tektonikus és fluviális hatások a Kőszegi-hegység és a Rába közti dombvidék kialakulásában [The role of tectonic and fluvial forces in the formation of the hilly area between Kőszeg Mountains and Rába River]. *Földtani Közlöny*, 143, 157–176 (in Hungarian with English abstract).
- Kovács, G., Telbisz, T., Székely, B. and Timár, G., 2014. DEM-derived markers of drainage network changes in the Eastern Alpine Foothills. *Journal of Maps*, 11, 255–260. <http://dx.doi.org/10.1080/17445647.2014.948938>
- Lantos, M. and Hámor, T., 1989. A fúrás magnetosztatográfiai értékelése [Magnetostatigraphic evaluation of the borehole]. In: Gőgh, Zs. (ed.). *A Szombathely-II. sz. fúrás földtani eredményei* [Geological results of Szombathely-II borehole]. Drilling report. Hungarian Geological Institute, 714–722 (in Hungarian).
- Lowrie, W., 2007. *Fundamentals of Geophysics* Cambridge University Press, pp 374.
- Magyar, I., Lantos, M., Ujszászi, K. and Kordos, L., 2007. Magnetostatigraphic, seismic and biostratigraphic correlations of the Upper Miocene sediments in the northwestern Pannonian Basin System. *Geologica Carpathica*, 58, 277–290.
- Magyar, I., Radivojević, D., Sztanó, O., Synak, R., Ujszászi, K. and Pócsik, M., 2013. Progradation of the paleo-Danube shelf margin across the Pannonian Basin during the Late Miocene and

- Early Pliocene. *Global and Planetary Change*, 103, 168–173. <http://dx.doi.org/10.1016/j.gloplacha.2012.06.007>
- Marple, R. and Talwani, P., 2000. Evidence for a buried fault system in the Coastal Plain of the Carolinas and Virginia — implications for neotectonics in the southeastern United States. *Geological Society of America Bulletin*, 112, 200–220. [http://dx.doi.org/10.1130/0016-7606\(2000\)112<200:EFABFS>2.0.CO;2](http://dx.doi.org/10.1130/0016-7606(2000)112<200:EFABFS>2.0.CO;2)
- Nash, D. B. and Beaujon, J. S., 2006. Modeling degradation of terrace scarps in Grand Teton National Park, USA. *Geomorphology*, 75, 400–407. <http://dx.doi.org/10.1016/j.geomorph.2005.07.027>
- Nebert, K., 1979. Die Lignitvorkommen Südburgenlands. *Jahrbuch der Geologischen Bundesanstalt*, 122, 143–180 (in German).
- Pascher, G. A., 1999. Geologische Karte des Burgenlandes. 1:200 000. Geologischen Bundesanstalt, Wien.
- Peacock, D. C. P. and Sanderson, D. J., 1994. Geometry and Development of Relay Ramps in Normal Fault System. *AAPG Bulletin*, 78, 147–165.
- Pelletier, J., DeLong, S., Al-Suwaidi, A., Cline, M., Lewis, Y., Psillas, J. and Yanites, B., 2006. Evolution of the Bonneville shoreline scarp in west-central Utah: Comparison of scarp-analysis methods and implications for the diffusion model of hillslope evolution. *Geomorphology*, 74, 257–270. <http://dx.doi.org/10.1016/j.geomorph.2005.08.008>
- Petit, C. and Mouthereau, F., 2012. Steep topographic slope preservation by anisotropic diffusion: An example from the Neogene Têt fault scarp, eastern Pyrenees. *Geomorphology*, 171–172, 173–179. <http://dx.doi.org/10.1016/j.geomorph.2012.05.016>
- Ratschbacher, L., Behrmann, J. and Pahr, A., 1990. Penninic windows at the end of the Alps and their relation to the intra-Carpathian basins. *Tectonophysics*, 172, 91–105.
- Reches, Z., 1978. Analysis of Fault in three-dimensional strain field. *Tectonophysics*, 47, 109–129.
- Royden, L. H. and Horváth, F., 1988. The Pannonian basin. A Study in Basin Evolution. *American Association of Petroleum Geologist Memoir*, 45, 117–145.
- Ruszkiczay-Rüdiger, Zs., Fodor, L. I. and Horváth, E., 2007. Neotectonics and Quaternary landscape evolution of the Gödöllő Hills, Central Pannonian Basin, Hungary. *Global and Planetary Change*, 58/1–4, 181–196. <http://dx.doi.org/10.1016/j.gloplacha.2007.02.010>
- Ruszkiczay-Rüdiger, Zs., Fodor, L., Horváth, E. and Telbisz, T., 2009. Discrimination of fluvial, eolian and neotectonic features in a low hilly landscape: a DEM-based morphotectonic analysis in the Central Pannonian Basin, Hungary. *Geomorphology*, 104/3–4, 203–217. <http://dx.doi.org/10.1016/j.geomorph.2008.08.014>
- Sanchez, G., Rolland, Y., Corsini, M., Braucher, R., Bourlès, D., Arnold, M. and Aumaître, G., 2010. Relationships between tectonics, slope instability and climate change: Cosmic ray exposure dating of active faults, landslides and glacial surfaces in the SW Alps. *Geomorphology*, 117, 1–13. <http://dx.doi.org/10.1016/j.geomorph.2009.10.019>
- Scheingross, J. S., Minchew, B. M., Mackey, B. H., Simons, M., Lamb, M. P. and Hensley, S., 2013. Fault-zone controls on the spatial distribution of slow-moving landslides. *Geological Society of America Bulletin*, 125/3–4, 473–489. <http://dx.doi.org/10.1130/B30719.1>
- Schmid, S. M., Fügenschuh, B., Kissling, E. and Schuster, R., 2004. Tectonic map and overall architecture of the Alpine orogen: *Eclogae Geologicae Helvetiae*. 97/1, 93–117.
- Schönlaub, H. P., 1973. Schwamm-Spiculae aus dem Rechnitzer Schiefergebirge und ihre stratigraphische Wert: *Jahrbuch der Geologischen Bundesanstalt*, 116, 34–49.
- Schönlaub, H. P., 2000 (ed.). *Geologie der österreichischen Bundesländer. Burgenland. Erläuterungen zur Geologischen Karte des Burgenlandes 1 : 200.000*. Geologische Bundesanstalt, Wien, Austria, 130 pp.
- Singleton, J. S., 2013. Development of extension-parallel corrugations in the Buckskin-Rawhide metamorphic core complex, west-central Arizona. *Geological Society of America Bulletin*, 125/3–4, 453–472. <http://dx.doi.org/10.1130/B30672.1>
- Štěpančíková, P., Dohnal, J., Pánek, T., Lój, M., Smolková, V. and Šilhán, K., 2011. The application of electrical resistivity tomography and gravimetric survey as useful tools in an active tectonics study of the Sudetic Marginal Fault (Bohemian Massif, central Europe). *Journal of Applied Geophysics*, 74, 69–80. <http://dx.doi.org/10.1016/j.jappgeo.2011.03.007>
- Szentgyörgyi, K. and Juhász, Gy., 1988. Sedimentological characteristics of the Neogene sequences in SW Transdanubia, Hungary. *Acta Geologica Hungarica*, 31, 209–225.
- Sztanó, O., Szafián, P., Magyar, I., Horányi, A., Bada, G., Hughes, D.W., Hoyer, D.L. and Wallis, R.J., 2013. Aggradation and progradation controlled clinothems and deepwater sand delivery model in the Neogene Lake Pannon, Makó Trough, Pannonian Basin, Hungary. *Global and Planetary Change*, 103, 149–167. <http://dx.doi.org/10.1016/j.gloplacha.2012.05.026>
- Tari, G., 1994. *Alpine Tectonics of the Pannonian basin*. PhD Thesis, Rice University, Texas, pp. 501.
- Tari, G., 1996. Extreme crustal extension in the Rába river extensional corridor (Austria/Hungary). *Mitteilungen der Gesellschaft der Geologie- und Bergbaustudenten Österreichs*, 41, 1–18.
- Tari, G., Horváth, F. and Rumpler, J., 1992. Styles of extension in the Pannonian Basin. *Tectonophysics*, 208, 203–219.
- Telbisz, T., Kovács, G., Székely, B. and Szabó, J., 2013. Topographic swath profile analysis: a generalization and sensitivity evaluation of a digital terrain analysis tool. *Zeitschrift für Geomorphologie*, 57/4, 485–513. <http://dx.doi.org/10.1127/0372-8854/2013/0110>
- Vendel, M., 1973. *Skizze des geologischen Aufbaues der Stadt Sopron und ihrer Umgebung (W-Ungarn)*. Publication of the Geological Institute of Hungary MÁFI, Budapest, pp. 28.
- Wilkins, S. J. and Schultz, R. A., 2003. Cross faults in extensional settings: Stress triggering, displacement localization, and implications for the origin of blunt troughs at Valles Marineris, Mars. *Journal of Geophysical Research, Planets*, 108/E6, 5056. <http://dx.doi.org/10.1029/2002JE001968>

Winterer, E.L., Metzler, C.V. and Sarti, M., 1991. Neptunian dykes and associated breccias (Southern Alps, Italy and Switzerland): role of gravity sliding in open and closed systems. *Sedimentology*, 38, 381–404.

Zovoili, E.; Konstantinidi, E. and Koukouvelas, I. K., 2004. Tectonic Geomorphology of escarpments: the cases of Kompotades and Nea Anchialos faults. *Bulletin of Geological Society of Greece*, 36, 1716–1725.

Received: 9 September 2014

Accepted: 13 August 2015

Gábor KOVÁCS<sup>1)2)3)\*)</sup>, László FODOR<sup>4)</sup>, Szilvia KÖVÉR<sup>4)</sup>, Gábor MOLNÁR<sup>4)</sup>, Donát RAÁB<sup>1)</sup>, Tamás TELBISZ<sup>5)</sup> & Gábor TIMÁR<sup>1)</sup>

<sup>1)</sup> Department of Geophysics and Space Sciences, Eötvös University, H-1117 Budapest, Pázmány Péter sétány 1/C, Hungary;

<sup>2)</sup> Department of Geology, University of West Hungary, H-9700 Szombathely, Károlyi Gáspár tér 4., Hungary;

<sup>3)</sup> Geomega Ltd., H-1095 Budapest, Mester utca 4., Hungary;

<sup>4)</sup> MTA-ELTE Geological, Geophysical and Space Science Research Group, Hungarian Academy of Sciences at Eötvös University, H-1117 Budapest, Pázmány Péter sétány 1/C, Hungary;

<sup>5)</sup> Department of Physical Geography, Eötvös University, H-1117 Budapest, Pázmány Péter sétány 1/C, Hungary;

<sup>\*)</sup> Corresponding author, skovacs.gabor@caesar.elte.hu